

Altered rRNA processing disrupts nuclear RNA homeostasis via competition for the poly(A)-binding protein Nab2

Lisbeth-Carolina Aguilar^{1,†}, Biplab Paul^{2,†}, Taylor Reiter³, Louis Gendron⁴, Arvind Arul Nambi Rajan⁵, Rachel Montpetit⁶, Christian Trahan¹, Sebastian Pechmann⁴, Marlene Oeffinger^{1,4,7,*} and Ben Montpetit^{2,3,5,6,*}

¹Department for Systems Biology, Institut de recherches cliniques de Montréal (IRCM), Montréal, QC, Canada, ²Department of Cell Biology, University of Alberta, Edmonton, Canada, ³Food Science Graduate Group, University of California Davis, Davis, CA, USA, ⁴Département de biochimie et médecine moléculaire, Université de Montréal, Montréal, QC, Canada, ⁵Biochemistry, Molecular, Cellular and Developmental Biology Graduate Group, University of California Davis, Davis, CA, USA, ⁶Department of Viticulture and Enology, University of California Davis, Davis, CA, USA and ⁷Division of Experimental Medicine, McGill University, Montreal, QC, Canada

Received May 26, 2020; Revised October 06, 2020; Editorial Decision October 07, 2020; Accepted October 12, 2020

ABSTRACT

RNA-binding proteins (RBPs) are key mediators of RNA metabolism. Whereas some RBPs exhibit narrow transcript specificity, others function broadly across both coding and non-coding RNAs. Here, in *Saccharomyces cerevisiae*, we demonstrate that changes in RBP availability caused by disruptions to distinct cellular processes promote a common global breakdown in RNA metabolism and nuclear RNA homeostasis. Our data shows that stabilization of aberrant ribosomal RNA (rRNA) precursors in an *enp1-1* mutant causes phenotypes similar to RNA exosome mutants due to nucleolar sequestration of the poly(A)-binding protein (PABP) Nab2. Decreased nuclear PABP availability is accompanied by genome-wide changes in RNA metabolism, including increased pervasive transcripts levels and snoRNA processing defects. These phenotypes are mitigated by overexpression of PABPs, inhibition of rDNA transcription, or alterations in TRAMP activity. Our results highlight the need for cells to maintain poly(A)-RNA levels in balance with PABPs and other RBPs with mutable substrate specificity across nucleoplasmic and nucleolar RNA processes.

INTRODUCTION

In eukaryotes, such as the yeast *S. cerevisiae*, both non-coding (ncRNA; e.g. snoRNA and rRNA) and protein coding messenger RNAs (mRNA) are synthesized and processed in the nucleus as part of the gene expression program. Each transcript associates with a set of RNA-binding proteins (RBPs) as ribonucleoprotein particles (RNPs) wherein the RBPs guide different processing events (1–3). During biogenesis, RNPs are surveyed by quality control mechanisms to decay aberrantly processed RNAs, ensuring that these transcripts do not continue along the gene expression pathway (3–6). Consequently, competition between biogenesis and surveillance factors for maturing transcripts within the nucleus is thought to be critical for determining transcript fate (e.g. decay versus maturation and export) and shaping the overall cellular transcriptome (7,8).

The RNA exosome constitutes a central part of the gene expression system that maintains cellular RNA homeostasis (7–10). At its core, the RNA exosome is a 10 subunit complex that harbors RNA binding and nuclease activities used to carry out RNA biogenesis and quality control, including Dis3/Rrp44, which possesses both exo- and endonuclease functions (11,12). The nuclear RNA exosome also contains an eleventh subunit, Rrp6, which is a 3'-5' exonuclease (13–15). In addition, the Trf4/5-Air1/2-Mtr4 polyadenylation (TRAMP) and Nrd1/Nab3/Sen1 (NNS) complexes support RNA exosome-mediated RNA processing and decay activities by targeting RNA substrates to the

*To whom correspondence should be addressed. Tel: +1 530 752 5955; Fax: +1 530 752 0382; Email: benmontpetit@ucdavis.edu
Correspondence may also be addressed to Marlene Oeffinger. Tel: +1 514 987 5668; Fax: +1 514 987 5532; Email: marlene.oeffinger@ircm.qc.ca
†The authors wish it to be known that, in their opinion, the first two authors should be regarded as Joint First Authors.
Present address: Biplab Paul, Gastrointestinal Unit, Massachusetts General Hospital, Boston, MA, USA.

RNA exosome (16–21). Through nuclease-associated activities, and in conjunction with the TRAMP and NNS complexes, the RNA exosome participates in both the biogenesis and surveillance of different classes of RNAs, including ribosomal RNA (rRNA), small nucleolar RNAs (snoRNAs), and mRNAs (9,10,22,23). Consequently, when RNA exosome activity is lost, or TRAMP and/or NNS functions are abolished, RNA biogenesis and surveillance is severely perturbed, resulting in the stabilization of various RNA processing intermediates (16,17,20,21,24–27). For example, precursor rRNA (pre-rRNA) species and 3'-extended snoRNAs accumulate due to stalled or defective processing events in RNA exosome, TRAMP, and NNS mutants, with aberrant transcripts localizing to discrete subdomains of the nucleus (14,20,28–35).

Loss of nuclear RNA surveillance activity also leads to the stabilization of other types of transcription products collectively referred to as pervasive transcripts. Based on the mutant background in which they were originally detected, pervasive transcripts have been classified into various groups, including cryptic unstable transcripts (CUTs) and stable unannotated transcripts (SUTs) in a *rrp6Δ* mutant (21,36), and Nrd1 unterminated transcripts (NUTs) in a *nrd1Δ* mutant (37). In addition, loss of another exonuclease involved in RNA processing and decay, Xrn1, results in the stabilization of a related class of transcripts termed XUTs (38). Both CUTs and NUTs undergo transcriptional termination via the NNS complex similar to snRNAs and snoRNAs (17,27,37,39,40). However, most SUTs and XUTs are terminated by the cleavage and polyadenylation factor (CPF) pathway, with SUTs being degraded through activities of the RNA exosome, nonsense-mediated decay (NMD) pathway, and Xrn1, while XUTs are generally exported and degraded in the cytoplasm by Xrn1 (38,41). These data collectively highlight the fact that biogenesis and decay of different classes of RNAs are facilitated by overlapping machineries (e.g., RNA exosome, NNS, and TRAMP complex), which include shared RBPs.

Recent genome-wide studies have identified RBP substrates and revealed that specific RBPs besides the RNA surveillance machinery also interact with several different RNA classes (42,43). One such RBP was Nab2, a poly(A)-binding protein (PABP). Nab2 is known to bind nuclear mRNAs to protect them from decay and facilitate export to the cytoplasm (44–48), but was also found to bind pervasive and RNA polymerase III transcripts (42,49). This ability of Nab2 to associate with different types of RNA suggests that competition must occur between different transcript classes for Nab2. Thus, changes in the amount of Nab2 engaged in one pathway (i.e., RNA surveillance and decay) could limit the availability of Nab2 to function in other processes (i.e., RNA biogenesis and export). Indeed, previous work has shown that mutations in RNA exosome subunits result in an accumulation of both poly(A)-RNA and Nab2 within the nucleolus (31,35). Similarly, accumulation of Nab2 on nuclear mRNAs upon nuclear export failure has been shown to leave nascent transcripts vulnerable to nuclear decay (44,45). These data suggest that alterations in RNA biogenesis and surveillance that produce stable nuclear poly(A)-RNAs may compete for Nab2; however, de-

spite these observations, the underlying mechanisms and the species of polyadenylated and accumulated RNAs has so far remained unidentified.

Recently, loss of Enp1, a ribosome biogenesis factor not previously implicated in RNA surveillance and decay, was shown to cause phenotypes shared with RNA exosome mutants that included mRNA, poly(A)-RNA and RBP (e.g. Nab2) accumulation in a sub-nuclear domain (35). Enp1 is required for 40S subunit maturation and export to the cytoplasm (50,51). It binds to the 3' end minor domain of the 20S pre-ribosomal RNA (rRNA), a precursor to the mature 18S rRNA, close to site D in the Internal Transcribed Spacer 1 (ITS1), where, together with Ltv1 and Tsr1, it coordinates stabilization of the pre-40S ribosomal beak structure in its immature conformation, facilitates repositioning of the ribosomal protein S3 (Rps3 or uS3) and late integration of Rps10 (eS10) (52–54). Loss of protein function in the *enp1-1* temperature sensitive (*ts*) mutant inhibits early rRNA processing, synthesis of 20S pre-rRNA, and production of mature 40S ribosomal subunits (51,54). Disruption of the Ran exchange factor Srm1 (Prp20), which functions in nucleocytoplasmic transport (55), similarly causes poly(A)-RNA and mRNA accumulation in a sub-nuclear domain (35). This raises the question of how the shared phenotypes of poly(A)-RNA accumulation and RBP sequestration can arise in cells carrying mutations in distinct pathways, such as RNA surveillance, ribosome biogenesis, and nucleocytoplasmic transport, and whether they represent a common cellular state at the molecular level.

In this study, we demonstrate that disruptions in pre-rRNA processing caused by *enp1-1*, or loss of RNA exosome function via *csf4-ph*, lead to association of Nab2 with pre-rRNAs, snoRNAs, and the ribosomal processing machinery, resulting in sequestration of Nab2 away from its normal nuclear interactome. In addition, *enp1-1* cells show genome-wide changes in the expression of mRNAs and pervasive transcripts that are correlated with changes in RNA exosome mutants (e.g. *rrp6Δ*, *dis3-1* and *csf4-ph*), as well as having shared snoRNA processing defects. These and other supporting data suggest a model in which: (i) aberrant pre-rRNAs (i.e. incorrectly processed or stalled in the processing pathway) generated in an *enp1-1* mutant compete for and limit Nab2 availability; (ii) decreased Nab2 activity leads to the generation and stabilization of nuclear RNA surveillance substrates; (iii) a buildup of surveillance substrates further limits the availability of Nab2 and other RBPs; and, (iv) the accumulation of substrates caused by both the loss of *enp1-1* and RBP sequestration saturates the nuclear RNA exosome causing a terminal phenotype in *enp1-1* cells similar to that of an RNA exosome mutant. In line with this model, overexpression of Pab1, a PABP known to rescue viability of a *nab2Δ* mutant (47), reduced the observed *enp1-1* phenotypes and enhanced the growth of *enp1-1* cells at a semi-permissive temperature. Overall, these data support a mechanism by which accumulation of excess aberrant nucleolar RNA, both polyadenylated and non-polyadenylated, disrupts nuclear RNA homeostasis through sequestration of Nab2 and limiting PABP activity.

MATERIALS AND METHODS

Yeast strain growth

Yeast strains and plasmids used in this study are listed in Supplementary Tables S4 and S5. Cells were grown in YPD or synthetic complete media lacking the appropriate amino acid to maintain plasmids when appropriate. All transformations were carried out using high-efficiency LiAc/SS-DNA/PEG protocol (56). Unless noted otherwise, cells for RNA-based or protein-based analyses were isolated, rapidly frozen in liquid nitrogen, and cryolysis was performed by solid phase milling in a planetary ball mill (Retsch) producing a fine cell grindate (57). All grindate was stored at -80°C until processed either for affinity purification or RNA extractions.

Fluorescent *in situ* hybridization (FISH)

Fluorescent *in situ* hybridization (FISH) was performed using 2 ng of TYE 563 labeled LNA oligo-dT (Exiqon Inc., Woburn, MA) per sample. Briefly, yeast strains were grown at room temperature until $\text{OD}_{600} = 0.8$, transferred to 37°C for 90 min if necessary, and fixed by adding 37% formaldehyde (Sigma-Aldrich) directly to the culture to a 5% final concentration. Cells were fixed at the growth temperature (e.g. room temperature or 37°C) for 15 min, centrifuged at 3300 RCF for 1 min, and the cell pellet washed two times with buffer A (0.1 M potassium phosphate pH 6.5 and 0.5 mM MgCl_2). To remove the yeast cell wall, cells were resuspended with 250 μl of buffer B (0.1 M potassium phosphate pH 6.5, 0.5 mM MgCl_2 , and 1.2 M Sorbitol) supplemented with beta-mercaptoethanol (Fisher) to 0.4% and Zymolase at 0.02 mg/ml followed by incubation at 37°C for 35 min. After spheroplasting, the cell pellet was collected by centrifugation at 400 RCF for 3 min and re-suspended in 200 μl of buffer B. Cells were placed on poly-L-lysine coated 8-well glass slides and incubated at room temperature for 10 min. Un-adhered cells were removed by washing two times with buffer A, followed by permeabilization in ice-cold methanol for 6 min and ice-cold acetone for 30 s, after which slides were allowed to air dry. Prior to hybridization, the hybridization solution (10 \times saline-sodium citrate (SSC), 10 \times Denhardt's solution, and 0.02% Tween 20) without probe was added to each well and incubated at 37°C for 2 h and then replaced with hybridization solution containing probes and incubated at 37°C for at least 12 h. The following day, cells were washed sequentially with 2 \times SSC, 1 \times SSC, 0.5 \times SSC for 30 min, and 2 \times phosphate buffered saline (PBS) for 10 min at room temperature. After the final wash, slides were dipped into 100% ethanol for 10 s, air-dried, and mounting media (Vectorlabs) with 4',6-diamidino-2-phenylidole (DAPI) was applied to each sample and a coverslip was affixed. Imaging was performed on an Andor Dragonfly imaging system using a Leica DMi8 microscope and an Andor iXon Ultra 888 EMCCD camera driven by Fusion software using a 60 \times 1.4 N.A. oil objective. Image analysis was performed in FIJI (58).

Imaging GFP fusions with FISH

Yeast strains carrying integrated or plasmid expressed GFP reporters were grown in selective media overnight, trans-

ferred to YPD for 2 h, and then shifted to 37°C for the indicated time. Following temperature shift, cells were fixed for 15 min using 2% paraformaldehyde and then processed for FISH and imaged as described.

Nab2 affinity purification

All strains were harvested in log phase ($\text{OD}_{600} = \sim 0.8$), transferred to 37°C for 90 min if required, and cell pellets were snap frozen in liquid nitrogen for grindate generation by cryo-milling (57). Nab2-PrA RNP purifications along with negative controls (PrA-tag expressed alone) were performed in RNP buffer (20 mM HEPES-KOH pH 7.4, 110 mM KOAc, 0.5% triton X-100, 0.1% Tween-20, 4 $\mu\text{g}/\text{ml}$ pepstatin A, 180 $\mu\text{g}/\text{ml}$ phenylmethylsulfonyl fluoride, 1:5000 antifoam A) supplemented with 100 mM NaCl (RNP100) as previously described (59). Briefly, 0.5 g of cell grindate was resuspended in 4.5 ml of RNP100 buffer and homogenized by polytron. Lysates were cleared by centrifugation at 2465 RCF, 4°C for 10 min and subsequently incubated with 3.75 mg IgG-conjugated Dynabeads, pre-washed in RNP100, for 30 min at 4°C on a rotating wheel. After ten washes in RNP100, detergents were removed by washing the bead-bound complexes in 0.1 M $\text{NH}_4\text{OAc}/0.1$ mM MgCl_2 . After a final wash in 20 mM Tris-HCl pH 8.0, on-bead digestion of the isolated complexes was performed in 20 mM Tris-HCl pH8.0 at 37°C (59). The digestion was stopped by adding formic acid to a final concentration of 2%.

Mass spectrometry

LC-MS/MS analysis. Tryptic peptides were cleaned using C18 ZipTips as per supplier recommendations (Millipore). For LC-MS, each sample was injected to near saturation of the signal, while an equivalent volume of their respective negative controls were injected.

Liquid chromatography was performed using a PicoFrit fused silica capillary column (15 cm \times 75 μm i.d.; New Objective, Woburn, MA, USA), self-packed with C-18 reverse-phase resin (Jupiter 5 μm particles, 300 \AA pore size; Phenomenex, Torrance, CA, USA) using a high-pressure packing cell on the Easy-nLC II system (Proxeon Biosystems, Odense, Denmark) and coupled to the LTQ Orbitrap Velos (ThermoFisher Scientific, Bremen, Germany) equipped with a Proxeon nanoelectrospray Flex ion source. 0.2% formic acid (Solvent A) and 100% acetonitrile/0.2% formic acid (Solvent B) were used for chromatography and peptides were loaded on-column at a flowrate of 600 nl/min and eluted with a three slope gradient at a flowrate of 250 nl/min. Solvent B was first increased from 2 to 25% over 20 min, then from 25 to 45% over 40 min, and finally from 45 to 80% B over 10 min.

The mass spectrometer was operated in data-dependent mode (DDA) with a locked mass (371.101233 Da) using the following settings. Full scan acquisition was carried out in the Orbitrap at a resolution of 60 000 (at m/z of 400). The top 16 most abundant precursors were selected, fragmented using CID (normalized collision energy of 35 V and activation q of 0.25 for 10 ms), and acquired in the linear ion trap in parallel. Mass over charge ratio range was set at 400–1800 for MS scanning with a target value of 1 000 000 charges,

and from $\sim 1/3$ of parent m/z ratio to 2000 for MS/MS with a target value of 10 000 charges. Data dependent scan events used a maximum ion fill time of 100 ms and 1 microscan. Capillary temperature was set to 250°C, while nanospray and S-lens voltages were set to 1.3–5171.7 kV and 50 V, respectively. Precursors were dynamically excluded for 22 s, after two counts occurring within 21.5 s.

Protein identification. The peak list files were generated with Proteome Discoverer (version 2.1.0.81) using the following parameters: minimum mass set to 500 Da, maximum mass set to 6000 Da, no grouping of MS/MS spectra, precursor charge set to auto, and minimum number of fragment ions set to 5. Protein database searching was performed with Mascot 2.5 (Matrix Science) against the NCBI *S. cerevisiae* protein database (20160802). The mass tolerances for precursor and fragment ions were set to 10 ppm and 0.6 Da, respectively. Trypsin was used as the enzyme allowing for up to one missed cleavage. Cysteine carbamidomethylation was specified as a fixed modification, and methionine oxidation as variable modifications. Data analysis was performed using Scaffold (version 4.8.4).

Mass spectrometry data analysis. Protein and peptide identification thresholds in Scaffold™ were set to 95% and 90% which resulted in respective decoy false discovery rates of 3.4% and 0.59%. Exclusive spectrum counts (ESC) were used for semi-quantification of protein preys, and mass spectrometry results were analyzed as previously described (60). Briefly, only Exclusive Spectral Counts (ESCs) above background detected in negative controls were retained (Supplementary Tables S2 and S3). To take protein size into account in the quantification, preys with at least five ESCs in both replicates were normalized against the number of theoretical peptides each protein generate by *in silico* digest. The theoretical trypsin digestion was performed using MS-digest (<http://prospector.ucsf.edu>) with zero missed cleavages, no variable modifications, and a minimum of seven amino acids per peptide within a mass range of 718–4000 Da. The obtained values were finally normalized against the value of the bait protein in each experiment (Supplementary Tables S2 and S3). Low confidence interactors are listed as grey values (Supplementary Table S3).

RNA sequencing

All code related to RNA-seq analyses has been deposited at: https://github.com/montpetitlab/Aguilar_and_Paul_et_al_2020.

RNA extraction for Ribo-depleted and dT-enriched analyses. All strains were grown to log phase ($OD_{600} = \sim 0.8$), transferred to 37°C for 90 min if required, and cell pellets were snap frozen in liquid nitrogen for grindate generation by cryo-milling (57). RNA extractions were performed using 5 mg of cryo-ground cell powder thawed in Trizol and purified on a RNeasy column (74104, Qiagen). All kits were used as per supplier specifications. The RNA extracts were either Poly(A)-RNA enriched via oligo-dT (E7490, NEB) or ribo-depleted (MRZY1324, Epicentre) and cDNA libraries were

prepared using the Kapa stranded RNA-seq library preparation kit (Kapa Biosystems). Paired end 50 (PE50) RNA-sequencing was performed using a HiSeq 2500.

Genome and transcriptome preparation. For transcript quantification, all libraries were quantified against the same transcriptome using Salmon (version 0.12.0) (61). The custom transcriptome was prepared using a bed file that contained coordinates for pervasive transcripts, ribosomal RNAs, and mRNAs to obtain transcript fasta sequences using *bedtools getfasta* command (version 2.29.2) against the UCSC sacCer3 genome (62,63). For RPKM estimation, all libraries were aligned to the UCSC sacCer3 genome.

Ribo-depleted and dT-enriched RNA-seq analysis. Paired-end reads were trimmed using Trimmomatic (version 0.39) to quality trim and remove adapters (64). Trimmed reads were quantified against the custom transcriptome using *Salmon quant* (61). A count matrix was generated using the tximport R package (version 1.14.0) (65). Differential expression was performed using the R package DESeq2 (version 1.26.0) using the *DESeq* function and specifying a wald test (66). For ribo-depleted analyses, three biological replicates from *csl4-ph* and two from *rrp6Δ*, *dis3-1*, *enp1-1*, *srm1-ts* and control strains were used. All mutants were contrasted against control to generate $\log_2(\text{FC})$ values for each transcript. To generate the correlation matrix, the R *cor* function using pearson's correlation was used. $\log_2(\text{FC})$ values were also used to plot accumulation curves, heatmaps, snoRNA, and mRNA class information from (42). For dT-enriched analyses, three biological replicates from *csl4-ph* and control strains, and two from *enp1-1* and *srm1-ts* strains were used. $\log_2(\text{FC})$ values were used to plot snoRNA and rRNA changes relative to control, and mRNA class information from (42).

To quantify differences in alignment depth and position to snoRNA genes, trimmed reads were also aligned against the UCSC sacCer3 genome using hisat2 (version 2.1.0) (67). These bam alignment files were sorted and indexed using samtools (version 1.10) (68). Data for snoRNA profiles and heatmaps were generated using deeptools (version 3.3.2) (69). First, the deeptools *bamCoverage* command was used with parameter *-normalizeUsing RPKM*. Then, the *computeMatrix* command with parameters *scale-regions* was used to generate RPKM estimates across all snoRNA genes in conjunction with a snoRNA bed file from (62). Results were visualized using the *plotHeatmap* command and in R. To quantify differences in alignment depth and position to snoRNA genes, the same procedure was followed with both ribo-depleted and dT-enriched libraries.

3' Tag-seq preparation and analysis. All strains were grown in selective media until $OD_{600} = 0.8$, transferred to 37°C for 90 min, and 5.0 ODs of cells were harvested by centrifugation and snap frozen on liquid nitrogen. RNA was extracted using the Quick-RNA Fungal/Bacterial prep kit (Zymo Research). Samples were treated with DNAase I (Zymo Research) on column and RNA integrity was assessed by 2% gel electrophoresis. Library preparation and sequencing was carried out by UC Davis Genome Center following the 3'-Tag Sequencing method (QuantSeq 3'

mRNA-Seq kits) using an Illumina HiSeq 4000 with single end 90 bp reads.

The first 12 reads were trimmed per manufacturer instructions using Trimmomatic (version 0.38) (64). Poly(A) tails and adapters were removed using the bbMap command *bbduk.sh* (version 38.20) (70). Trimmed reads were quantified against the custom transcriptome using *Salmon quant* (61). A count matrix was generated using the tximport R package (version 1.14.0) (65), and by selection the *counts* dataframe from the tximport object, as 3' Tag-seq data should not be normalized for transcript length given that reads originate from the 3' end of the transcript. Differential expression was performed using the R package DESeq2 (version 1.26.0) using the *DESeq* function and specifying a wald test (66). All contrasts were performed against control and within mutants when appropriate. Log₂(FC) values were used to plot accumulation curves for pervasive transcripts and mRNA classes information from (42).

Northern blot analysis

Total RNA extractions were performed from flash-frozen cell pellets using a hot phenol RNA extraction (71). Poly(A)-RNA was enriched from 770 µg of total RNA using PolyATtract mRNA Isolation Systems as per supplier specifications (Z5310, Promega). RNA associated with Nab2-PrA complexes were recovered by affinity purification, as detailed above, but with the following modifications: 1g cell grindate and 7 mg IgG-conjugated Dynabeads were incubated in RNP100 buffer supplemented with 0.2 U/µl RNasin. Post incubation, beads were washed six times in RNP100. Finally, RNA was extracted from bead-bound complexes using phenol/chloroform/IAA (24:24:1).

For northern blotting, 3 µg of total RNA was loaded for each sample. Volume equivalents for input and FT samples were also loaded. RNA was resolved on a 1% agarose-formaldehyde gel in Tricine-Triethanolamine and transferred onto a nylon membrane in 10× SSC by capillary force as previously described (72). 10 pmol of each oligonucleotide was radioactively labelled with 20 µCi of [^γP32]-ATP (3000 Ci/mmol; Perkin-Elmer), cleaned using G25 columns as per supplier specifications (GE Healthcare, 27-5325-01) and incubated with the nylon membrane to detect different RNA species (for probe sequences, see Supplementary Table S6). The probes were hybridized overnight at 37°C in 50 ml Hybridization Buffer (6× SSPE (6 mM EDTA/0.894 M NaCl/60mM phosphate buffer pH 7.4), 5× Denhardt's, 0.2 mg/ml single-stranded DNA and 0.2% SDS). Membranes were washed at 37°C for 15 min in 50 ml 6× SSPE. For yU14 and snR30, two successive 50 ml washes were carried out with 5× SSPE, 0.1% SDS followed by one wash with 0.5× SSPE, 0.1% SDS. Membranes were exposed to phosphor imaging screens, which were scanned on a Typhoon (FLA 9500) after 1–4 days of exposure.

Liquid growth assay

Cell cultures were grown overnight to stationary phase in selective media then diluted to an OD₆₀₀ of 0.2 in a 48-well plate. Strains were grown for 18 h with shaking at 32°C and OD₆₀₀ measurements were taken using a NEO2 plate reader

(BioTek, USA). A line was fit to the growth curve to determine the maximum growth rate over a continuous 90-min period for each strain within the 18 h of growth.

Statistics

The statistical tests used are defined within the methods sections, figures, and/or figure legends, including exact *P*-values, *t*-values, and degrees of freedom where applicable.

RESULTS

enp1-1 and *srml1-ts* transcriptomes are similar to RNA exosome mutants

In *S. cerevisiae*, the disruption of multiple genes functioning in distinct biological processes, including RNA surveillance (*RRP6*, *DIS3* and *CSL4*), rRNA processing (*ENP1*), and nucleocytoplasmic transport (*SRM1*), share a common set of phenotypes that includes the accumulation of poly(A)-RNA in a sub-nuclear domain (31,35). Previous work has indicated that in RNA exosome mutants this poly(A)-RNA mass is associated with the nucleolus (31,35). To better understand the mechanism behind poly(A)-RNA accumulation, we first characterized the transcriptome in these *ts* mutant strains. RNA-seq analyses were performed on ribosome-depleted (ribo-) RNA samples prepared from control, *rrp6Δ*, *dis3-1*, *csl4-ph*, *enp1-1* and *srml1-ts* strains after 90 min at 37°C when poly(A)-RNA accumulation was apparent (Figure 1A). Analysis of the RNA-seq data showed that within the control strain ~85% of reads were generated from mRNAs and the remaining ~15% from ncRNAs, which included snRNAs, snoRNAs and pervasive transcripts (Supplementary Figure S1a and Supplementary Table S1). In the mutants, the number of reads generated from mRNA decreased (~75–82%), while ncRNA reads increased, largely due to augmented levels of pervasive transcripts (~12–19%). Cluster analysis of log₂ fold change relative to control indicated that these mutants displayed similar patterns of gene expression, with mRNAs significantly reduced and pervasive transcripts increased (Figure 1B, Supplementary Figure S1b and c). For pervasive transcripts, no one class (e.g. CUTs, SUTs, NUTs or XUTs) was specifically impacted, with the various types of pervasive transcripts all showing increased levels in the mutants assayed (Supplementary Figure S1c). Correlated changes in gene expression between *rrp6Δ*, *dis3-1*, *csl4-ph*, *srml1-ts* and *enp1-1* mutants were also apparent in correlation coefficient scores calculated between RNA exosome mutants or between RNA exosome and *enp1-1* or *srml1-ts* mutants (Figure 1C).

Aiming to further the role of RBPs in mRNA metabolism, recent work has defined ten broad classes of RBP interaction profiles with mRNA (42), with each class considered indicative of differences in mRNA processing. For example, class I-III mRNAs are bound by specific RBPs in a pattern similar to pervasive transcripts that are targeted by the RNA exosome for degradation. In contrast, class IV-X are bound by RBPs in a pattern that suggests these transcripts are exported, translated, and decayed in the cytoplasm. To understand if the relative abundance of mRNA transcripts in the five *ts* mutants correlated with

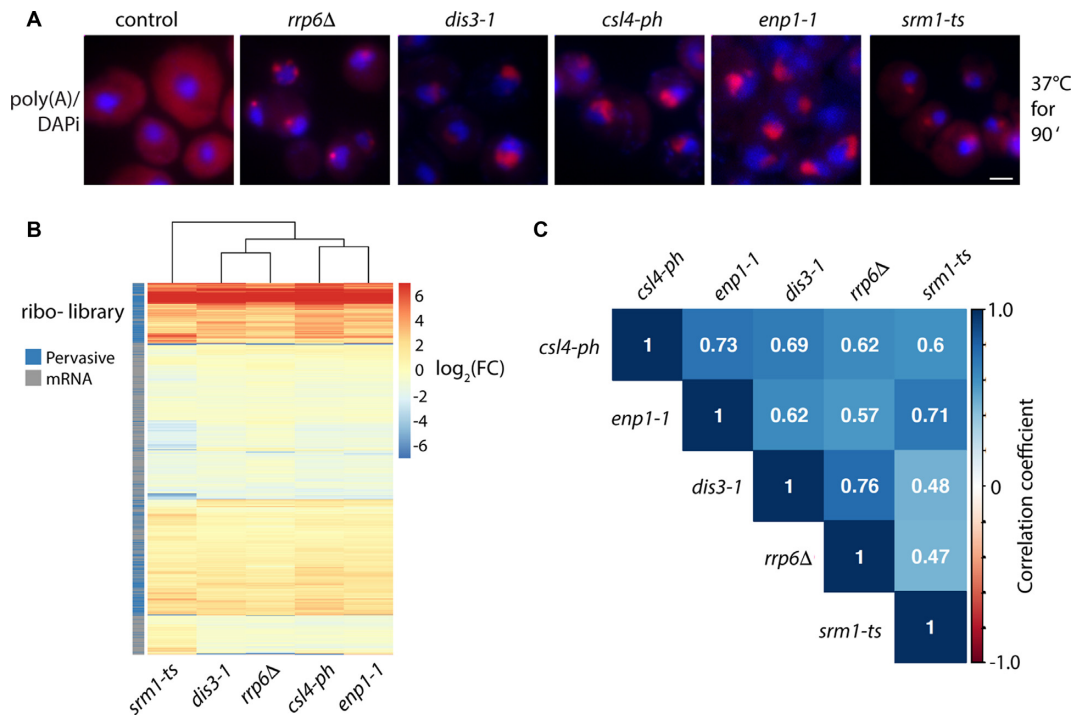


Figure 1. Transcriptomes in RNA decay and ncRNA processing mutants are similar. (A) FISH images showing nuclear accumulation of poly(A)-RNA in control, *rrp6Δ*, *dis3-1*, *csl4-ph*, *enp1-1* and *srm1-ts* cells after 90 min of growth at 37°C. Nucleus shown in blue (DAPI) and poly(A)-RNA in red. Scale bar = 2 μm. (B) Hierarchical clustering of genes significantly differently expressed at $P < 0.01$, $\log_2(\text{FC})$, in *ts* mutant strains after 90 min at 37°C with respect to control in ribo-depleted RNA libraries. Bar on the left indicates transcript identity, mRNA (gray) and pervasive transcripts (blue) with each row representing an individual transcript and each column a mutant. Red shades indicate positive and blue negative value changes in gene expression. $\log_2(\text{FC})$ values greater than the absolute value of 6 are encoded as maximum saturation. (C) Correlation matrix displaying calculated correlation coefficients of transcriptome-wide $\log_2(\text{FC})$ between strains after 90 min at 37°C in ribo-depleted RNA libraries. For B and C, $\log_2(\text{FC})$ values correspond to the average from at least two biological replicates using all reads quantified against each feature.

RBP interaction profiles, expression changes within each mRNA class were plotted for each mutant. This analysis revealed that mRNAs in classes I-III were expressed at higher levels in the mutants than in the control strain, which included meiotic transcripts known to be targeted for decay by the RNA exosome in vegetative cells (73), while mRNAs in class IV-X trended lower (Supplementary Figure S2). Together, the stabilization of class I-III mRNAs and pervasive transcripts are suggestive of lowered nuclear surveillance and/or RNA-decay activity in *srm1-ts* and *enp1-1* mutants, similar to *rrp6Δ*, *dis3-1* and *csl4-ph* cells.

csl4-ph and *enp1-1* cells accumulate polyadenylated ncRNA

The shared phenotypes and transcriptomic profiles of *rrp6Δ*, *dis3-1*, *csl4-ph*, *enp1-1* and *srm1-ts* mutants suggest that the poly(A)-RNA signal observed by fluorescent in situ hybridization (FISH) in these cells could arise from stabilized pervasive transcripts and nuclear mRNAs (Figure 1 and Supplementary Figure S1); however, it remains unknown which transcripts are actually polyadenylated in these cells. To characterize polyadenylated transcripts, RNA-seq was performed using oligo-dT-purified RNA from *csl4-ph*, *enp1-1* and *srm1-ts* strains after 90 min at 37°C and compared to control (Supplementary Table S1). In control cells, dT-enrichment resulted in ~88% of reads being mapped to mRNAs and ~9% mapping

to pervasive transcripts (i.e. SUTs and XUTs) known to be polyadenylated (38,41). The remaining ~3% of reads mapped to rRNAs, which may be indicative of polyadenylated rRNA precursors generated during rRNA biogenesis (30). In the case of *csl4-ph* and *enp1-1*, the fraction of reads mapping to pervasive transcripts increased ~2-fold, similar to what was observed in ribo-depleted RNA libraries (Supplementary Table S1). The number of reads mapping to ncRNA in dT-enriched samples from *csl4-ph* and *enp1-1* strains also increased. Notably, an increase of ~30- and ~3.5-fold in snoRNA reads were observed in *csl4-ph* and *enp1-1* cells, respectively, which was not seen in ribo-depleted RNA samples. In line with this, differential expression analysis demonstrated that a large fraction of snoRNAs were increased in the dT-enriched libraries from *csl4-ph* and *enp1-1* cells, but not in ribo-depleted libraries, while snoRNAs were generally decreased in the *srm1-ts* strain regardless of library preparation (Figure 2A). To further investigate the increase in polyadenylated snoRNAs in *csl4-ph* and *enp1-1*, reads per kilobase of transcript per million mapped reads (RPKM) were estimated for normalized windows across snoRNAs. The resulting metagene plots for both *enp1-1* and *csl4-ph* showed that normalized read depth was significantly higher within the gene body and downstream of the transcription end site (TES) in poly(A)-RNA-enriched data compared to control cells, in particular in *csl4-ph* cells, while ribo-depleted samples indicated only

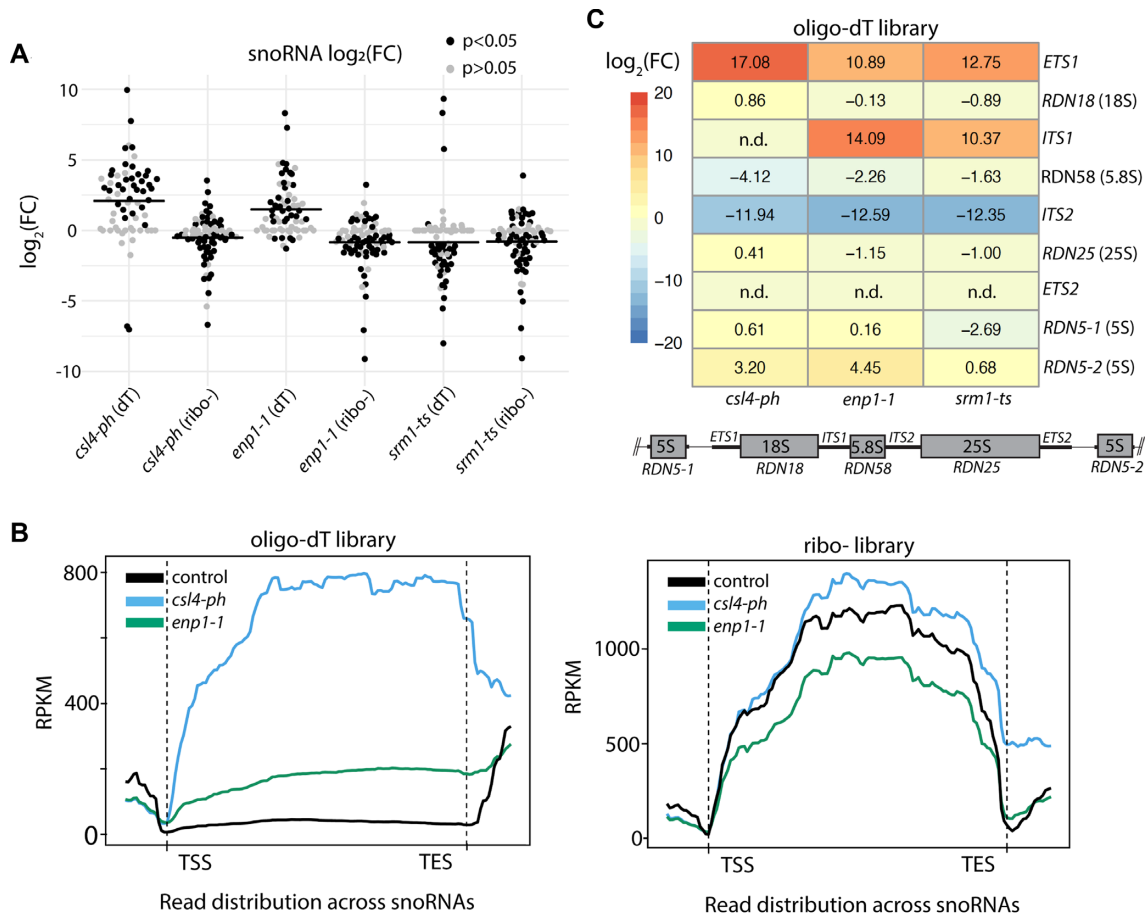


Figure 2. Polyadenylation of ncRNAs is increased in *Csl4* and *Enp1* mutants. (A) Plot displaying calculated $\log_2(\text{FC})$ values for snoRNAs in *csl4-ph*, *enp1-1* and *srm1-ts* cells after 90 min at 37°C with respect to control in both oligo-dT purified and ribo-depleted RNA libraries from at least two biological replicates. Average change across all transcripts is indicated by the solid line, dark circles indicate significance at $P < 0.05$, and gray dots were not significant at $P < 0.05$. (B) Metagenome analysis showing average read density across snoRNA genes in both oligo-dT purified (left) and ribo-depleted (right) RNA-seq libraries with respect to the transcription start site (TSS) and transcription end site (TES). Data is presented as RPKM, reads per kilo base per million mapped reads, to normalize for gene length and library size. (C) Heatmap displaying calculated $\log_2(\text{FC})$ values for rRNA transcripts generated from RDN25 (25S), RDN18 (18S), RDN58 (5.8S), and RDN5 (5S), plus associated transcribed spacers (*ETS1*, *ITS1*, *ITS2*, *ETS2*), within the rDNA locus (see schematic) in *csl4-ph*, *enp1-1* and *srm1-ts* cells after 90 min at 37°C with respect to control in oligo-dT purified RNA libraries. Transcripts that could not be calculated due to a lack of sufficient read counts are indicated as not determined (n.d.).

a minimal change in global snoRNA levels (Figure 2B). The differences in normalized read depth in ribo-depleted versus poly(A)-RNA-enriched libraries were also apparent for a large number of individual snoRNA genes (Supplementary Figure S3a). These data indicate that steady-state snoRNA levels do not significantly change in *csl4-ph* and *enp1-1* compared to control, but a significant fraction of snoRNAs are present as 3'-extended polyadenylated transcripts in *csl4-ph* and to a lesser extent in *enp1-1* cells. Given the known role of the RNA exosome in snoRNA processing (14,16,20,31,34,74–76), this was expected for *csl4-ph*, but not *enp1-1*, which has only been implicated in ribosome biogenesis (51,77).

To identify ribosomal precursor RNAs to which reads differentially mapped in *csl4-ph*, *enp1-1* and *srm1-ts* strains, we carried out differential expression analysis for defined rRNA regions. We observed a significant increase in the levels of the 5S rRNA gene variant, RDN5-2 (78), in *csl4-ph* and *enp1-1*, while levels of the RDN5-1 locus were

only marginally increased. The external transcribed spacer (*ETS1*; in *csl4-ph*, *enp1-1* and *srm1-ts*) and internal transcribed spacer (*ITS1*; in *enp1-1* and *srm1-ts*) regions of pre-rRNA were also highly elevated; however, the 18S rRNA (RDN18) region, which is located between *ETS1* and *ITS1*, was not (Figure 2C). In contrast, the regions coding for pre-60S subunit components (RDN58/5.8S rRNA; RDN25/25S rRNA) and the *ITS2* and *ETS2* regions showed a significant decrease across all mutants. These results suggest that changes in ncRNA biogenesis may be generating various polyadenylated pre-rRNA and snoRNA species that could represent an important fraction of the poly(A)-RNA signal detected by FISH in RNA exosome and *enp1-1* mutants (Figure 1A) and parallel previous reports of RNA exosome-dependent accumulation of specific polyadenylated ncRNA species (14,32,79).

In the case of *srm1-ts*, no large increases in rRNA or snoRNA reads were observed in the poly(A)-RNA-enriched sequencing data (Figure 2 and Supplementary Ta-

ble S1), suggesting that at the level of transcript polyadenylation the *srml1-ts* mutant is different from *csl4-ph* and *enp1-1* mutants. In line with this observation, the *srml1-ts* cells displayed the weakest poly(A)-RNA signal by FISH (Figure 1A). It is possible that these results reflect failed nucleocytoplasmic transport events, impacting the ability of nuclear proteins involved in directing (e.g. NNS complex) and performing (e.g. TRAMP complex) polyadenylation from accessing the nucleus. In support of this, both TRAMP (Trf4-GFP) and NNS (Nrd1-GFP) complex subunits were mainly localized to the cytoplasm and reduced in the nucleus of *srml1-ts* cells at 37°C (Supplementary Figure S3b). These data provide a plausible rationale for both the shared (pervasive transcript stabilization) and disparate (snoRNA polyadenylation) phenotypes of *srml1-ts* cells compared to *csl4-ph* and *enp1-1* cells.

The poly(A)-RNA-enriched RNA-seq data suggests that both *csl4-ph* and *enp1-1* cells accumulate pre-rRNA and snoRNA transcripts that are polyadenylated. To further determine ncRNA polyadenylation, total RNA versus oligo-dT purified RNA was analyzed by northern blotting using probes against pre-rRNAs, snoRNAs, and the *ACT1* mRNA as a control (see Supplementary Figure S4a for probe locations within the rRNA precursor). These data show that *dis3-1*, *csl4-ph*, *rrp6Δ* and *enp1-1* strains accumulated polyadenylated pre-rRNAs at 37°C (Figure 3A). Specifically, in *enp1-1* cells, polyadenylated forms of late (20S) and aberrant (23S, 21S, and 17S) pre-40S rRNAs (Figure 3A, lanes 5 versus 12 and Supplementary Figure S4b and c) were found to accumulate in accordance with a role for Enp1 in late 40S subunit maturation (26). Similarly, polyadenylated 40S precursors were increased in *csl4-ph* and *dis3-1* cells (Figure 3A, lanes 3 versus 10), pointing towards an inability to process and surveil pre-rRNAs due to the absence of RNA exosome components (30,80,81). Processing of 5.8S precursors was also impacted in *rrp6Δ*, and to a lesser extent in *csl4-ph* cells, as shown by the accumulation of polyadenylated 7S, 6S, and 5.8S+30 species (Figure 3A, lanes 3 versus 10 and 2 versus 9), in line with the known role of the RNA exosome and Rrp6 in 3'-end maturation of 5.8S rRNA (13). 5S rRNA was also found to be polyadenylated in *dis3-1*, *csl4-ph* and *rrp6Δ* cells, which may be caused by inefficient incorporation of the 5S rRNA into pre-60S subunits due to the processing defect in 60S maturation in these mutants (82). Even more prominent 5S polyadenylation was detected in *enp1-1* cells (Figure 3A, lanes 5 versus 12); while it is known that aberrant 90S and pre-40S assembly and processing events impact 60S maturation, including 5S rRNA incorporation, the detected 5S polyadenylation in *enp1-1* may also represent 5S rRNA transcripts produced from the RDN5-2 variant that were enriched in RNA-seq data (Figure 2C) (77,83). In comparison, no large increase in polyadenylated pre-rRNAs was observed in *srml1-ts* (Figure 3A, lanes 6 versus 13) or the mRNA export mutant *mex67-5* (Figure 3A, lanes 7 versus 14). In the case of snoRNAs, polyadenylated U14 and snR30 accumulated in *enp1-1* cells as well as in *dis3-1*, *csl4-ph*, and *rrp6Δ* (Figure 3A, lanes 5 versus 12), in accordance with the role of polyadenylation and the RNA exosome in snoRNA processing (34,84). These data, together with transcriptomic analyses, support the conclusion that there

is an increase in polyadenylated pre-ribosomal RNA and snoRNA species in both *enp1-1* and *csl4-ph* mutants.

Nab2 is associated with pre-rRNAs in *csl4-ph* and *enp1-1* mutants

The increased levels of aberrant ncRNA processing intermediates and subsequent localization of RBPs to the nucleolus in RNA exosome mutants (31,35) suggests that nucleolar ncRNA material may compete for RBPs and limit RBP activity in other RNA processing pathways. Nab2 is a nuclear poly(A)-binding protein (PABP), which was shown to primarily bind the poly(A)-RNA tail of nuclear mRNAs to protect them from decay and facilitate export to the cytoplasm (44–48); however, it was later found to also bind pervasive and RNA polymerase III transcripts (42,49). To test for interactions between Nab2 and specific transcripts, northern blot analyses were performed on RNA from Nab2-PrA purifications in control, *csl4-ph*, *enp1-1* and *srml1-ts* cells after a shift to 37°C. An enrichment of pre-rRNAs was observed with Nab2 in both *csl4-ph* and *enp1-1* cells compared to control. In particular, enrichment of 20S pre-rRNAs, the aberrant 21S, and 17S precursors, and 5S rRNA was detected in *enp1-1*, while 7S pre-rRNA was primarily observed in *csl4-ph* cells (Figure 3B, lanes 9 versus 10 and 12), which paralleled the major pre-rRNA species identified as polyadenylated in these mutants (compare Figure 3A and B). Hence, the purification of precursors from both ribosomal subunits indicates an association of Nab2 with both aberrant, and potentially polyadenylated, pre-40S and pre-60S complexes. Similarly, the snoRNAs U14 and snR30 associated with Nab2 in the mutant strains, but these were not the polyadenylated forms observed by northern blot using dT-enriched RNA (Figure 3A, lanes 9 and 12 versus Figure 3B, lanes 10 and 11), which may reflect mature snoRNAs associated with ribosome intermediates purifying with Nab2. Increased levels of *ACT1* pre-mRNA and mRNA were also found co-isolating with Nab2 (Figure 3B, lanes 10 and 11), matching the report of nuclear mRNA retention within the poly(A)-RNA sub-nuclear domain in the *enp1-1* mutant (35). Consistent with these interactions occurring in the nucleolus, both Nab2-GFP and the nucleolar protein Gar1-GFP co-localized with poly(A)-RNA in *csl4-ph* and *enp1-1* cells at 37°C (Figure 3C). In the case of *srml1-ts*, Nab2-GFP was largely cytoplasmic (Figure 3C), limiting access of Nab2 to nuclear mRNA and nuclear ncRNA transcripts, which is reflected by the lack of Nab2 binding to rRNA precursors below that of even control cells (Figure 3B, lane 9 versus 12). These results indicate that Nab2 is associated with ncRNA precursors, including polyadenylated and aberrant rRNA precursors and non-polyadenylated snoRNAs, in *csl4-ph* and *enp1-1* cells at 37°C.

To further explore the link between rRNA synthesis and the poly(A)-RNA and Nab2 localization phenotypes, control, *csl4-ph* and *enp1-1* cells were treated with rapamycin. Rapamycin was used here to limit production of pre-rRNAs by RNA Pol I and Pol III, and the generation of ribosomal protein mRNAs by RNA Pol II (85). FISH analysis showed that rapamycin treatment 15 min prior to the temperature shift prevented the poly(A)-RNA accumula-

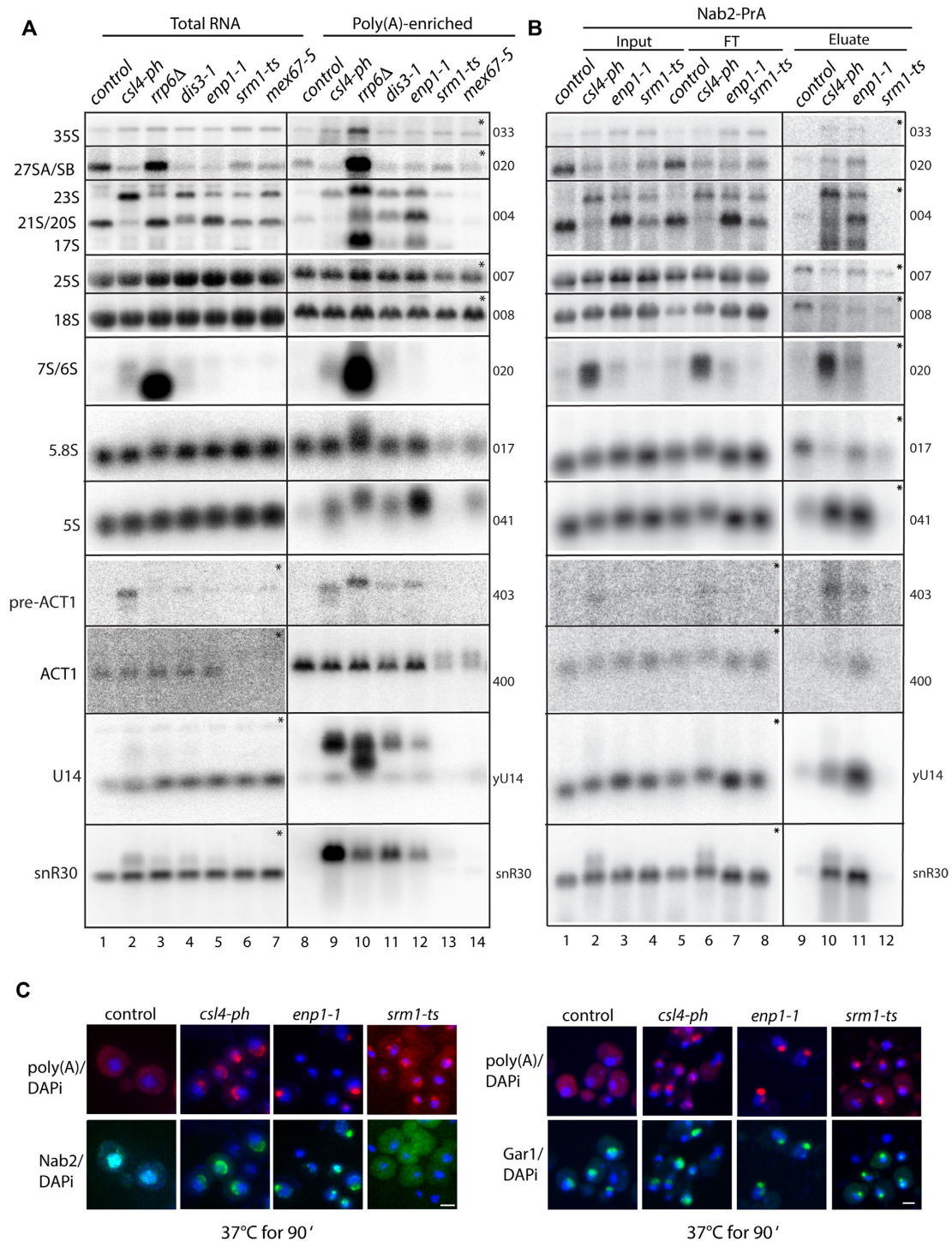


Figure 3. rRNA and snoRNA species are polyadenylated in *csl4-ph* and *enp1-1* mutants and polyadenylated pre-rRNAs associate with Nab2. (A) Total RNA was extracted from control, *csl4-ph*, *rrp6Δ*, *dis3-1*, *enp1-1*, *srm1-ts*, and *mex67-5* mutants after 90 min at 37°C. Poly(A)-RNA species were enriched from 770 μg of total RNA using oligo-dT and analyzed by northern blotting. Labeled oligonucleotide probes were used to detect indicated pre-rRNAs, rRNA processing intermediates, mature rRNAs, *ACT1* pre- and mature mRNAs, and snoRNAs (U14 and snR30). Probe numbers are listed beside each image and sequences are provided in Supplementary Table S6. (B) RNA species co-isolating with affinity-purified Nab2-PrA in control, *csl4-ph*, *enp1-1* and *srm1-ts* cells after 90 min at 37°C detected by northern blot analysis using indicated probes as in (A). Input material, flow through (FT), and Nab2 bound (eluate) samples are included for comparison. In A and B, panels marked with a * in the upper right hand corner were obtained following an extended exposure time. (C) Localization of plasmid expressed Nab2-GFP (pBM458) and Gar1-GFP (pBM547) compared to poly(A)-RNA detected by FISH in control, *csl4-ph*, *enp1-1*, and *srm1-ts* cells after 90 min at 37°C. Nucleus is shown in blue (DAPI), poly(A)-RNA in red, and the GFP-tagged fusion protein in green. Scale bar = 2 μm.

tion defect in both *csl4-ph* and *enp1-1* strains (Supplementary Figure S5a). In contrast, rapamycin treatment did not impact control cells or the mRNA export mutant *mex67-5* based on the number of cells scored to have a poly(A)-RNA accumulation phenotype. However, it was noted that the intensity of the nuclear poly(A)-RNA mass was generally lower in the *mex67-5* strain, which may relate to the lowered levels of ribosomal protein mRNAs upon rapamycin treatment (85). Under these conditions of rapamycin treatment with no obvious detectable poly(A)-RNA accumulation, Nab2-GFP localized throughout the nucleus in *csl4-ph* and *enp1-1* cells (Figure 4A). These observations are consistent with rRNA synthesis being a required component of both the poly(A)-RNA accumulation and nucleolar Nab2 sequestration phenotypes.

The purification of polyadenylated rRNA precursors with the PABP Nab2 and requirement for ongoing rRNA synthesis suggests that ncRNA polyadenylation could be involved in promoting the phenotypes observed in *csl4-ph* and *enp1-1* cells. If this is the case, a prediction would be that poly(A)-RNA accumulation and Nab2-GFP localization to the poly(A)-RNA mass would be dependent on TRAMP poly(A)-polymerase activity, which is responsible for pre-rRNA and snoRNA polyadenylation (20,26,28). Indeed, deletion of either of the genes encoding the TRAMP associated non-canonical poly(A)-polymerases, *TRF4* or *TRF5*, resulted in a strong reduction in the level of poly(A)-RNA detected in *enp1-1* cells and distribution of Nab2-GFP throughout the nucleus after 90 min at 37°C (Figure 4B). In the case of *csl4-ph*, double mutants with *trf4Δ* were not obtained, but *csl4-ph/trf5Δ* mutants similarly accumulated less poly(A)-RNA and showed a nuclear Nab2-GFP localization pattern (Figure 4B). Importantly, reintroduction of *Trf4-GFP* or *Trf5-GFP* in to *trf4Δ* or *trf5Δ* mutant strains resulted in poly(A)-RNA accumulation phenotypes (Supplementary Figure S5b). These findings indicate that polyadenylation by the TRAMP complex is required for both the poly(A)-RNA accumulation and Nab2-GFP nucleolar localization phenotypes observed in *csl4-ph* and *enp1-1* cells.

Nab2 interactome includes ribosome biogenesis factors in *csl4-ph* and *enp1-1* mutants

The observed nucleolar localization of Nab2 and increased association of Nab2 with ncRNAs suggests that Nab2 is engaged with a different set of nuclear machineries in *csl4-ph* and *enp1-1* strains. To characterize Nab2 associated proteins, affinity-purification mass spectrometry (AP-MS) was used to identify proteins enriched with Nab2-PrA purified from *csl4-ph* and *enp1-1* strains after 90 min at 37°C. As expected, AP-MS data from control samples revealed Nab2 interactions with proteins involved in nuclear mRNA processing, including proteins of the nuclear pore complex and mRNA export pathway (Supplementary Table S2 and S3). Nab2 isolated from *csl4-ph* cells retained most interactions compared to control cells, but also showed increased interactions with proteins involved in ribosome biogenesis (e.g. pre-40S and pre-60S) and ncRNA processing, including components of the NNS (e.g. Nab3, Nrd1, and Sen1) and TRAMP (e.g. Mtr4 and Trf4) complexes (Figure 5 and

Supplementary Table S2 and S3). In *enp1-1* cells, Nab2 interactome changes were even more pronounced; in particular, interactions with proteins of the nuclear pore complex and mRNA export pathway were lost, while interactions with ncRNA processing and ribosome biogenesis components were dominant. For example, Nab2 co-purified with the majority of the proteins of the small subunit (SSU) processome, which was also observed in *csl4-ph*, as well as components of H/ACA-type snoRNPs (e.g. Cbf5, Gar1p, Nhp2 and Nop10) that were unique to *enp1-1* cells.

Nab2 also showed repeatable differential interactions with subunits of the TRAMP complex in *enp1-1* (Mtr4, Trf5, and Air1) and *csl4-ph* (Mtr4, Trf4, and Air2) mutants (Supplementary Table S2 and S3). These differences may reflect the recently demonstrated role of the TRAMP5-1 complex (Trf5/Air1/Mtr4), in pre-rRNA degradation (86), as well as, a preference for performing surveillance of pre-40S rRNAs over pre-60S components and other ncRNAs and mRNAs (26,29,86). Finally, in *srm1-ts* cells, Nab2 interactions with the mRNA processing machinery and NPCs were generally reduced (Supplementary Table S3). A robust interaction was observed between Nab2 and Kap104, the karyopherin responsible for Nab2 nuclear import (87), which is consistent with a block in the nuclear import of Nab2-GFP in *srm1-ts* cells (Figure 3C). Overall, these data demonstrate a reorganization of the nuclear Nab2 protein interaction network in *enp1-1* and *csl4-ph* cells to include ribosomal processing pathways and other components involved in rRNA and snoRNA biogenesis that is consistent with Nab2 binding ncRNAs within the nucleolus.

Excess poly(A)-RNA alters nuclear RNA homeostasis and cellular fitness

Our accumulated data suggests a model in which loss of Enp1 leads to the stabilization of aberrant pre-rRNAs that bind Nab2 and promote further errors in RNA biogenesis (i.e. accumulation of mRNAs and pervasive transcripts) due to limited RBP availability. These disruptions to nucleolar pre-rRNA (*enp1-1*) and mRNA (e.g. Nab2 sequestration) processing appear to act in conjunction, producing an excess of substrates that overwhelms the nuclear RNA exosome. This model is supported by the finding that *enp1-1* cells exhibit a terminal phenotype similar to that observed in RNA exosome mutants (e.g. stabilized pervasive transcripts and snoRNA processing defects, see Figure 1B, Supplementary Figure S1, and Figure 2A, B). In such a scenario, the overexpression of Nab2 in *enp1-1* cells may buffer against excess nuclear poly(A)-RNA, disrupt this positive-feedback loop, and limit the development of RNA exosome-like phenotypes. To test this prediction, Nab2 was overexpressed exogenously from an inducible promoter to provide excess PABP activity. After 90 min at 37°C, overexpression of Nab2-GFP prevented the development of a poly(A)-RNA accumulation phenotype in *enp1-1* cells, but did not alter the phenotype of *csl4-ph* (Figure 6A). In contrast, cells that overexpressed GFP-Yra1, a non-poly(A)-binding RBP also recruited to the poly(A)-RNA mass in *csl4-ph* and *enp1-1* strains, or cells that carried an empty vector, retained the poly(A)-RNA accumulation phenotype in both mutant backgrounds (Figure 6B, C). These results are

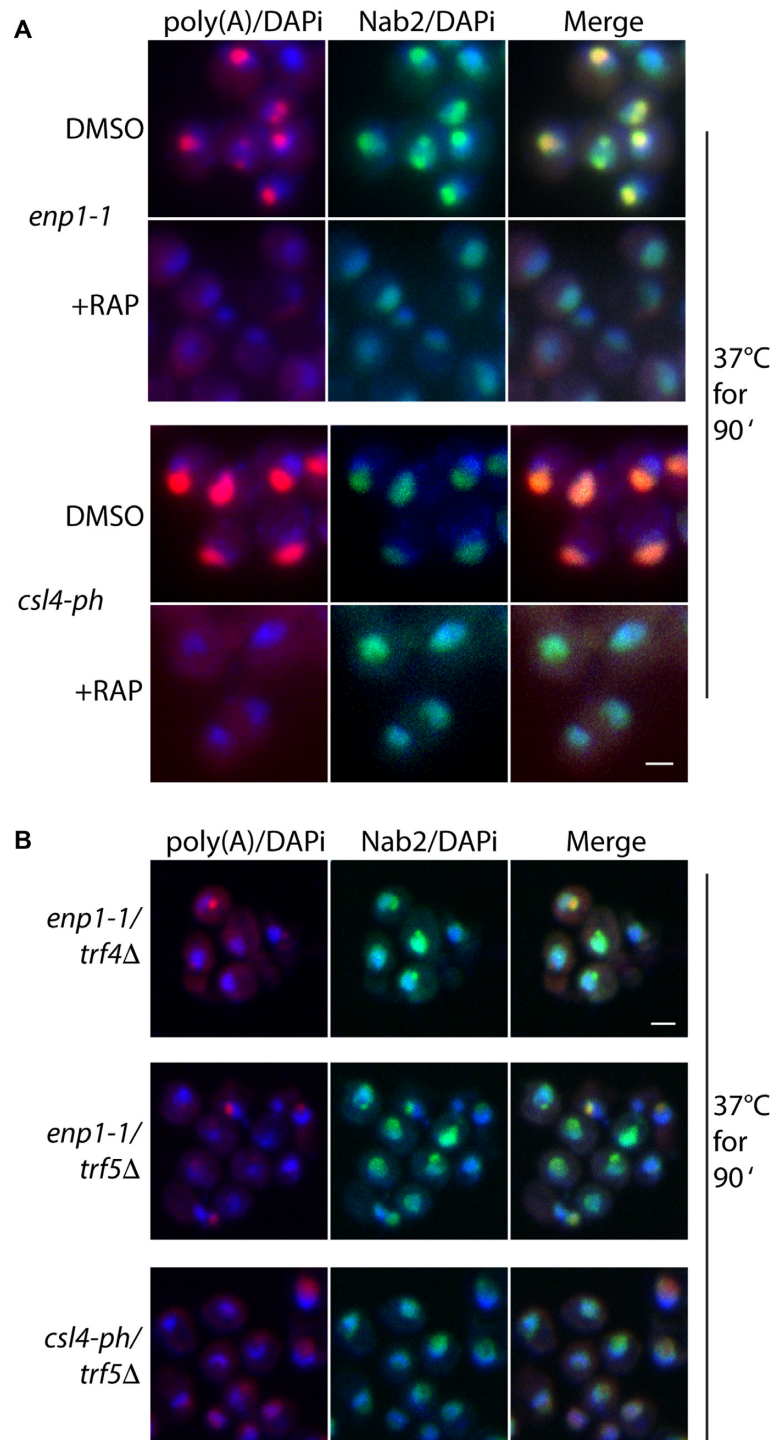


Figure 4. Poly(A)-RNA accumulation and Nab2 localization phenotypes are influenced by rRNA synthesis and TRAMP-dependent polyadenylation. (A) FISH image showing localization of poly(A)-RNA (red) and Nab2-GFP (green, expressed from the endogenous NAB2 locus) in control, *csl4-ph*, *enp1-1* strains 90 min at 37°C without (top, DMSO control) and with addition of rapamycin (bottom, 100 ng/ml rapamycin) 15 min prior to temperatures shift compared to DAPI (blue). (B) FISH image showing localization poly(A)-RNA (red) and Nab2-GFP (green, expressed from the endogenous NAB2 locus) in *enp1-1* with a *trf4Δ* or *trf5Δ* deletion or *csl4-ph* with a *trf5Δ* deletion after 90 min at 37°C as compared to DAPI (blue). Scale bars = 2 μm.

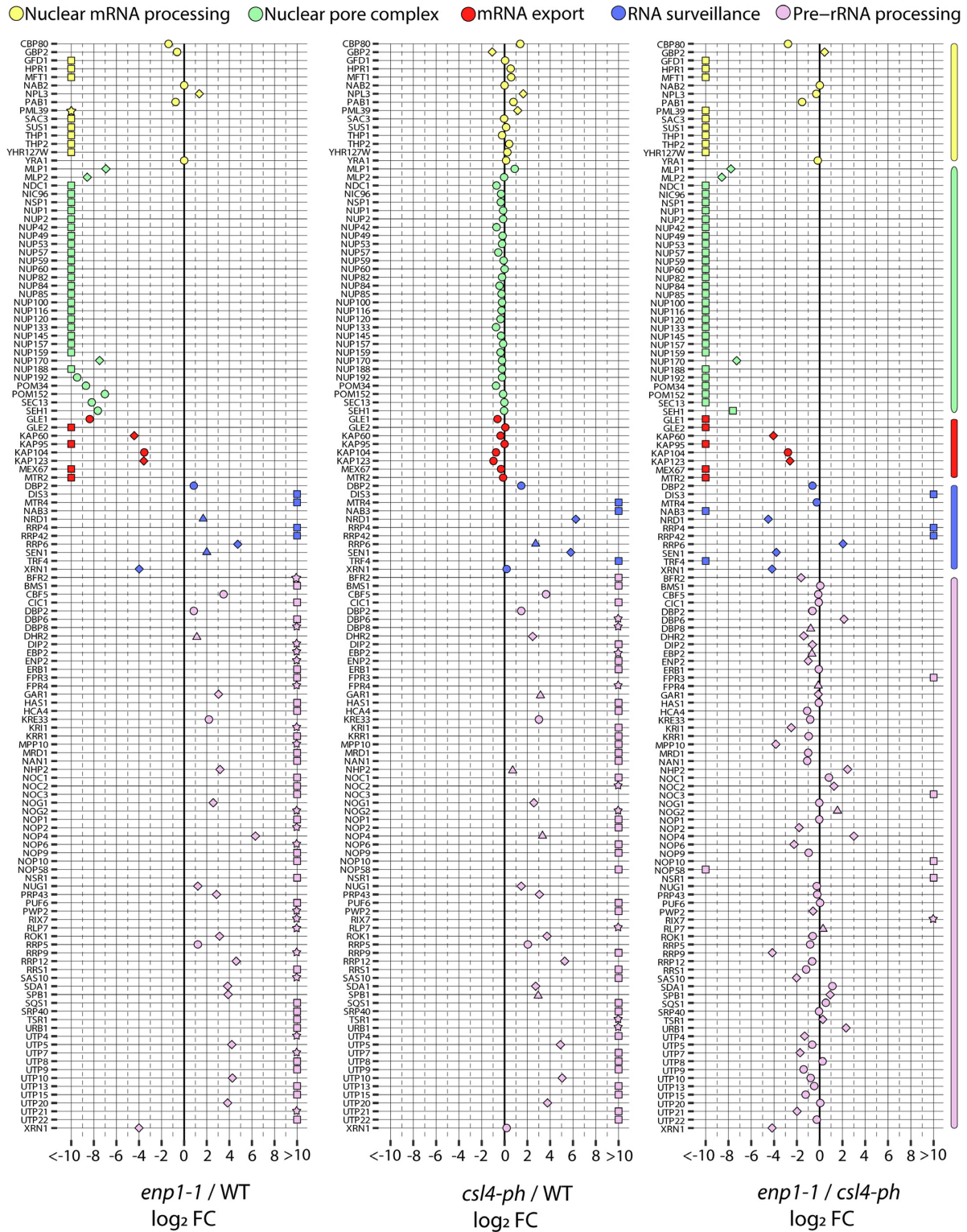


Figure 5. Nab2 protein interactions are altered in *csh4-ph* and *enp1-1* cells. Nab2-PrA associated proteins identified by AP-MS from control, *csl4-ph*, and *enp1-1* cells after 90 min at 37°C. Proteins were included if identified in at least one of the tested strains as a high confidence interaction (i.e., at least five exclusive spectrum counts (ESC) in two biological replicates). Each protein is presented as a colored shape, with the color indicating an associated biological process (see legend). Shapes are defined as follows: ● indicates a protein matching the defined high confidence criteria in both samples being compared; ◆ indicates a protein that was identified in both samples, but did not meet the high-confidence criteria in one of the samples being compared; ▲ indicates a protein identified in both samples, but at a level that is below the high-confidence criteria for both samples being compared; ■ indicates a protein identified in only one of the samples with high confidence; ★ indicates a protein identified in only one of the samples at a level below the defined criteria. Due to the inability to calculate a \log_2 (FC) in the cases where no peptides were identified (■ and ★), these data points are located to the extremes of the graph to indicate the fold change is >10 or <-10.

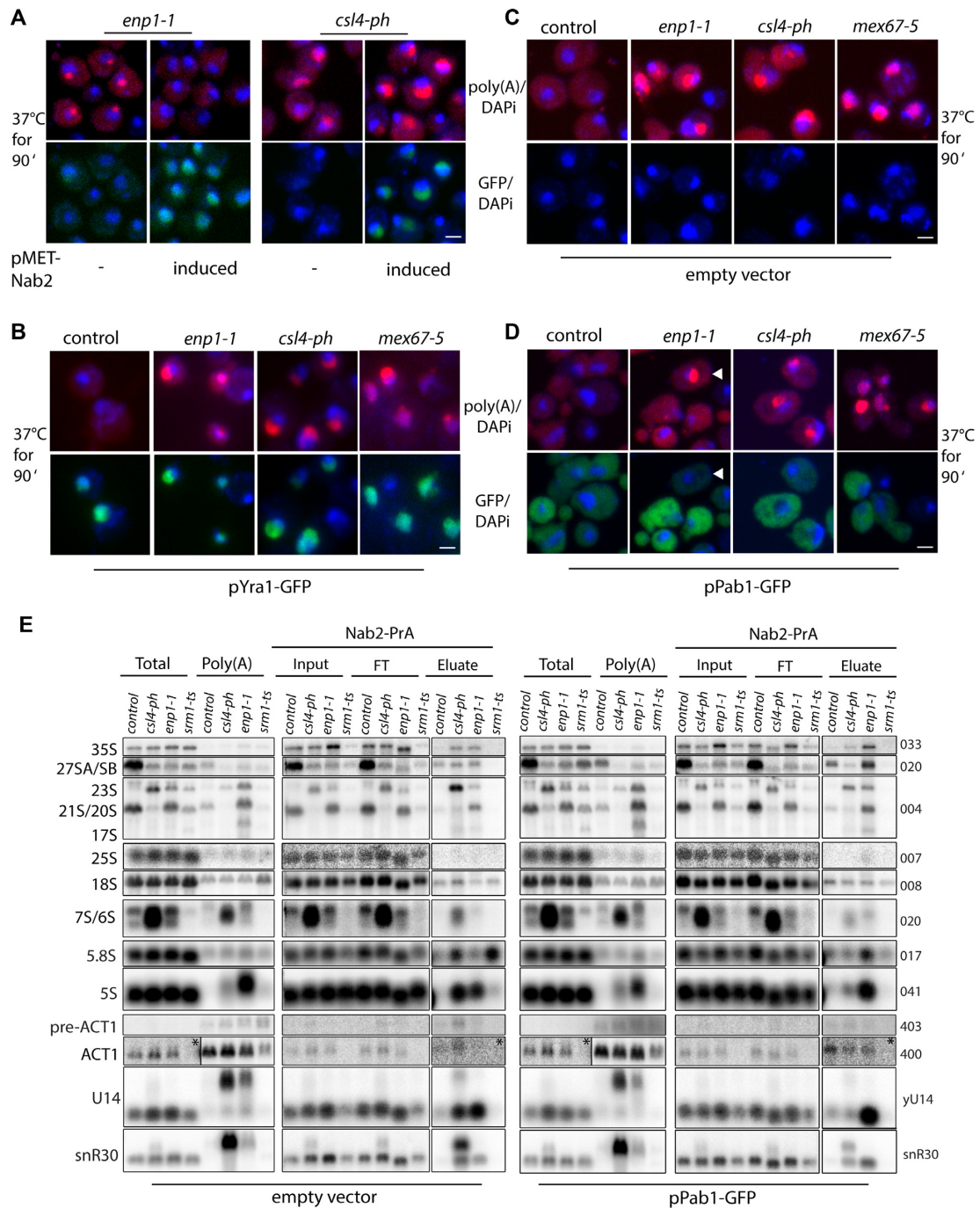


Figure 6. Poly(A)-RNA accumulation is decreased, but Nab2-ncRNA associations persist in an *enp1-1* strain overexpressing Pab1. (A) FISH image showing localization of poly(A)-RNA (red) in control, *csl4-ph*, *enp1-1*, and *mex67-5* strains with or without overexpression of Nab2-GFP (green) with respect to DAPI (blue) after incubation at 37°C for 90 min. Nab2-GFP expression was induced by removal of methionine from the growth media for 2 h prior to temperature shift. Scale bar = 2 μm. (B–D) FISH image showing localization of poly(A)-RNA (red) in control, *csl4-ph*, *enp1-1*, and *mex67-5* strains overexpressing Yra1-GFP (pBM763) or Pab1-GFP (pBM766) in green from a 2 μ-plasmid versus the empty plasmid control (pBM005) with respect to DAPI (blue) after incubation at 37°C for 90 min. In panel D, the arrowhead denotes a cell with low Pab1-GFP expression that also shows a poly(A)-RNA accumulation phenotype. Scale bars = 2 μm. (E) Northern blots showing total RNA, poly(A)-RNA, and RNA species co-isolating with affinity-purified Nab2-PrA extracted from control, *csl4-ph*, *enp1-1*, and *srm1-ts* cells overexpressing Pab1 (pBM874) from a 2 μ-plasmid versus an empty vector control (pBM007) after 90 min at 37°C. For the Nab2-PrA associated material, input material, flow through (FT), and Nab2 bound (eluate) samples are included for comparison. Probe numbers are listed beside each image and sequences are provided in Supplementary Table S6. Panels marked with a * in the upper right hand corner were obtained following an extended exposure time.

consistent with the proposed model suggesting that limited Nab2 activity is central to the development of a poly(A)-RNA phenotype in an *enp1-1* mutant.

Notably, it has been reported that the essential functions of Nab2 can be met when Pab1, another PABP, is overexpressed (47). In line with this, overexpression of Pab1-GFP from a 2 μ -plasmid (high copy plasmid) was similarly able to rescue the poly(A)-RNA accumulation phenotype in *enp1-1* (Figure 6D; note that Pab1-GFP expression is variable between cells using the 2 μ -plasmid system and cells with low/no expression retain the poly(A)-RNA accumulation phenotype as indicated in the figure panel). Overexpression of Pab1-GFP did not alter phenotypes in *csf4-ph* or the mRNA export mutant *mex67-5*, nor did the localization of Pab1-GFP obviously change in any of the tested strains. The ability of Pab1-GFP overexpression to rescue *enp1-1* phenotypes could be the result of Pab1 replacing Nab2 on polyadenylated RNAs that accumulate in this mutant or Pab1 fulfilling Nab2 cellular functions. To address the possibility that Pab1-GFP is displacing Nab2 from ncRNAs, northern analyses were again performed on RNA samples from Nab2-PrA affinity-purifications, as well as total and oligo-dT purified RNA, from cells shifted to 37°C for 90 min (Figure 6E). These data show that Pab1-GFP overexpression does not alter global rRNA processing in control cells or change the observed rRNA processing defects in any of the tested mutants, nor significantly decrease the interaction of Nab2 with pre-rRNAs in the *enp1-1* mutant. These data suggest that Pab1-GFP is suppressing *enp1-1* phenotypes by fulfilling Nab2-dependent PABP functions.

To investigate the effect of Pab1-GFP overexpression on nuclear RNA biogenesis, RNA-seq analyses were performed on RNA isolated from control, *enp1-1*, and *csf4-ph* strains overexpressing Pab1-GFP or carrying an empty vector control after 90 min at 37°C. Under conditions of excess Pab1-GFP, *enp1-1* cells had lower levels of pervasive transcripts and class I-III mRNAs (Figure 7A). In contrast, overexpression of Pab1-GFP had little impact on the levels of pervasive transcripts or mRNAs in *csf4-ph* cells. Pab1-GFP overexpression also reduced snoRNA processing defects as evidenced by a reduction in polyadenylated snoRNAs in *enp1-1* and *csf4-ph* strains (Figure 7B). These findings indicate that excess PABP activity is able to buffer the impact of an *enp1-1* mutation on global RNA processing and surveillance pathways.

Finally, if excess poly(A)-RNA is detrimental to cells and a catalyst of the phenotypes observed in *enp1-1* and *csf4-ph* mutants, it may be expected that excess PABP activity could improve the fitness of these strains at a semi-permissive temperature. Indeed, overexpression of Pab1-GFP improved the growth of both *enp1-1* and *csf4-ph* strains at 32°C, while having no impact on control or *mex67-5* cells (Figure 7C). Together these data strongly argue that limited PABP activity in response to alterations in pre-rRNA processing or changes in nuclear RNA surveillance impacts cellular fitness by disrupting nuclear RNA homeostasis.

DISCUSSION

RNA processing is mediated by specific RNA binding proteins (RBPs), some of which have been identified to interact

with several different classes of RNAs, whose levels need to be sufficient to ensure continued RNA metabolism (42,43). The findings reported here provide evidence that perturbation of RBP availability or activity (e.g. alterations in RNA surveillance, pre-rRNA processing, or nucleocytoplasmic transport) promotes a common global breakdown in nuclear RNA metabolism. For instance, the *srm1-ts* mutant appears to disrupt nuclear RNA homeostasis through limiting levels of RBPs in the nucleus, such as Nab2, TRAMP, and NNS complex subunits. In the case of *enp1-1*, specific defects in nucleolar rRNA processing result in excess of aberrant, including polyadenylated, pre-rRNAs that lead to sequestration of Nab2 and other RBPs in the nucleolus. In both scenarios, although the genetic lesion impacts functionally distinct pathways, it is the subsequent change in RBP availability that causes failures in RNA processing. These failures drive cells towards a set of shared terminal phenotypes, including a common cellular transcriptome defined by stabilized pervasive transcripts, aberrant pre-rRNAs, snoRNAs and the accumulation of nucleolar polyadenylated RNA.

PABPs and transcript specificity

Polyadenylation in eukaryotes has long been associated with mRNA processing leading to export, translation, and transcript stability (88–90), which is, in part, mediated by the PABPs that associate with the poly(A)-tail (91–94). Over time it has become clear that polyadenylation also occurs on ncRNAs, including rRNAs, sno/snRNAs, and pervasive transcripts, often directing their processing or decay by the RNA exosome (88,95). However, this raises the general issue of specificity, i.e. how is a poly(A)-tail on an mRNA distinguished from one on a ncRNA in order to direct differing outcomes. Context is likely very important, with events upstream of polyadenylation leading to specific RNP architectures (e.g. protein constituents), that when combined with other features such as transcript length, the polymerase involved and polyadenylation machinery used, would lead to differing outcomes. For example, transcript specificity was recently observed for different subsets of the TRAMP complex where binding specificity was conferred by the non-canonical poly(A) polymerases Trf4 and Trf5 (86). This supports the idea that the fate of a polyadenylated RNA may be influenced by the affinity it has for processing factors and vice versa. However, it is conceivable that this fate is also impacted by the sub-nuclear localization of a transcript, local RBP availability, and the overall kinetics of the processes involved (e.g. export versus nuclear decay). In the case of rRNA processing, it is likely the short and transient nature of poly(A)-tails added to pre-rRNA transcripts that is key to minimizing, or even preventing, their interaction with nuclear PABPs (20). However, given the extremely high level of rRNA production, stabilization of poly(A)-tracts on aberrant pre-rRNAs would be expected to have a strong influence on PABP availability, which may be well exemplified here by the phenotypes of an *enp1-1* mutant.

Under physiological conditions, regulated changes in RBP availability via stress-induced pathways are known to alter gene expression. For example, during heat shock Nab2 is phosphorylated and localized to nuclear foci, suggesting

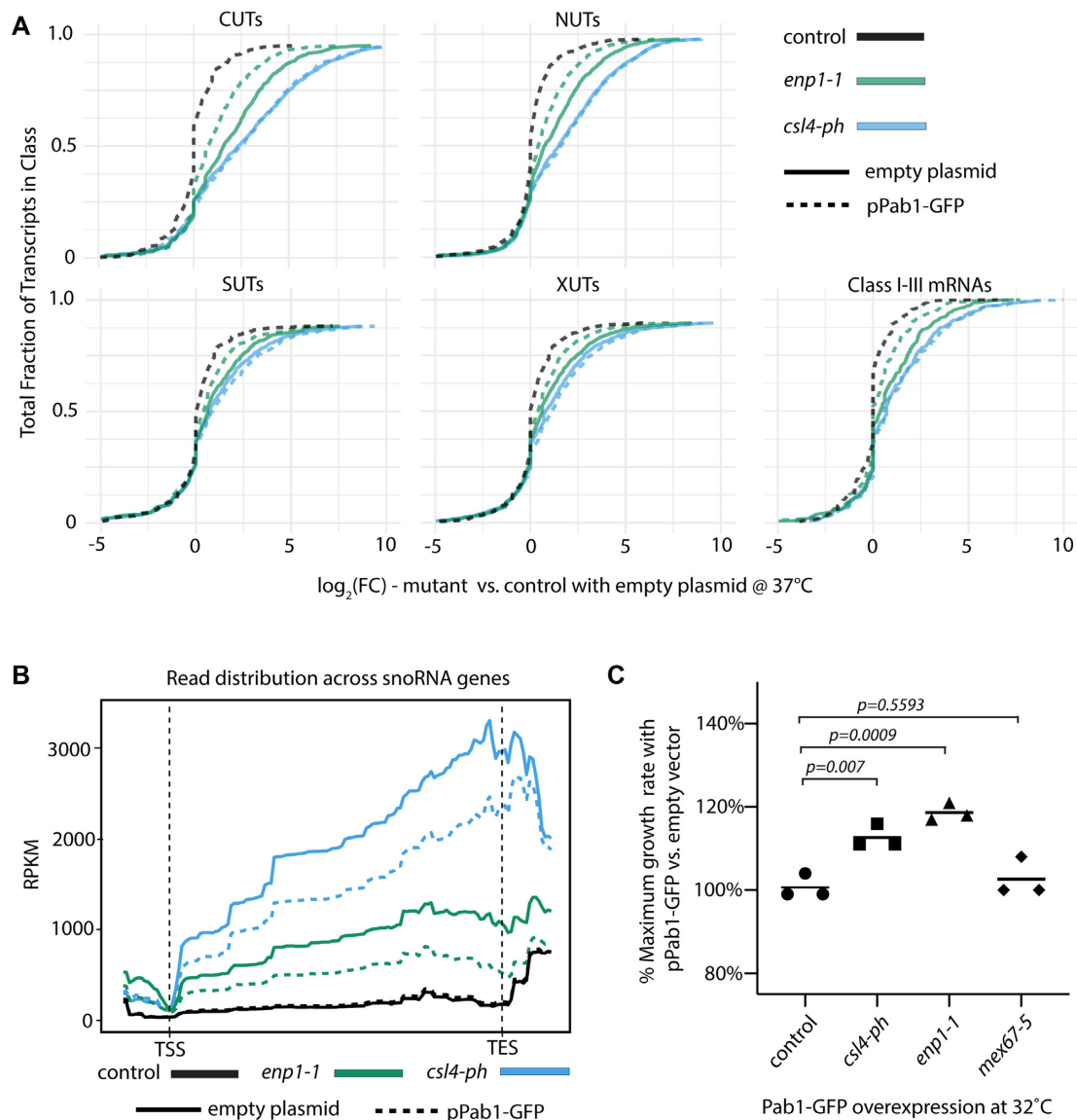


Figure 7. Excess PABP activity suppresses secondary *enp1-1* phenotypes. (A) Cumulative distribution plots of $\log_2(\text{FC})$ values for the indicated classes of transcripts observed for control (black lines), *csl4-ph* (blue lines), and *enp1-1* (green lines) strains overexpressing Pab1-GFP from a 2 μ -plasmid (pBM766, dashed lines) versus an empty vector control (pBM005, solid line). (B) Metagenome analysis showing average read density across snoRNA genes in control (black lines), *csl4-ph* (blue lines), and *enp1-1* (green lines) strains overexpressing Pab1-GFP from a 2 μ -plasmid (pBM766, dashed lines) versus an empty vector control (pBM005, solid line) with respect to the transcription start site (TSS) and transcription end site (TES). Data are presented as RPKM, reads per kilo base per million mapped reads, to normalize for gene length and library size. For both A and B, values were calculated using read data from three biological replicates as compared to the control strain with the empty plasmid as measured by 3'-TAG-RNA-seq. (C) Relative maximum growth rate of control, *csl4-ph*, *enp1-1*, and *mex67-5* strains in liquid culture when overexpressing Pab1-GFP (pBM766) from a 2 μ -plasmid at 32°C as compared to the same strains carrying an empty vector (pBM005). P-values for control versus *csl4-ph* ($P = 0.0070$, $t = 5.091$, and $df = 4$), control versus *enp1-1* ($P = 0.0009$, $t = 8.760$, and $df = 4$), and control versus *mex67-5* ($P = 0.5593$, $t = 0.6360$, and $df = 4$) were calculated from an unpaired *t*-test with a two-tailed distribution from three biological replicates.

that heat shock induces changes in Nab2 availability to alter mRNA export (96). In a similar way, it could be anticipated that a change in cellular state that causes alterations in mRNA or ncRNA processing would also feedback to impact genome-wide RNA maturation events through RBP availability. In agreement with this notion, recent work showed that stabilization of pervasive transcripts, such as CUTs in *rrp6* Δ cells, results in the sequestration of Nab3 and Nrd1 on these transcripts and titration of these RBPs

away from other RNA substrates resulting in genome-wide transcription termination defects due to limited NNS availability (97). Similarly, it was proposed that the accumulation of Nab2 on mRNAs upon nuclear export failure prevents its recycling to newly generated RNA molecules, which leaves nascent transcripts vulnerable to nuclear decay (44,45). Our work shows that an excess of aberrant pre-rRNAs can lead to a nucleolar sequestration of RBPs away from their customary nuclear RNA substrates resulting in a global imbal-

ance of RNA processing despite the presence of an intact surveillance system.

Our observations highlight the need for cells to maintain poly(A)-RNA levels in balance with PABPs and associated components across nuclear and nucleolar RNA machineries. Yet these data also demonstrates a mutable substrate specificity for some elements of the RNA processing machineries, in this case Nab2, across distinct RNA pathways and sub-nuclear regions. Recently, PAR-CLIP was used to establish transcriptome-wide binding maps for both RNA degradation and processing factors in yeast to determine their binding specificities for different classes of RNAs (43). While these factors may indeed have preferential binding for specific RNA classes under stable growth conditions, a certain degree of substrate flexibility and network plasticity seems to exist in order to maintain RNA homeostasis and, ideally, to counteract consequences of gene expression changes in response to intra- and extracellular cues or disturbances. However, as observed in the *enp1-1* strain, proteins not considered shared between RNA classes under normal conditions can show substrate mutability under certain circumstances with detrimental consequences for cells. Hence, a better understanding of the spatial and temporal regulation of polyadenylation and poly(A)-RNA binding by the various PABPs will be required to decipher how crosstalk between RNA processing and degradation machineries is regulated to modulate RNA homeostasis, without inciting scenarios where RBP-RNA interactions drive positive feed forward loops leading to lethal terminal phenotypes.

Enp1 and nuclear RNA homeostasis

Enp1 is a 40S ribosome biogenesis factor, one of few that is already present in the 90S complex and remains associated until late pre-40S biogenesis in the cytoplasm (50,51). It binds to the 3' end minor domain of the pre-18S rRNA, close to site D in the Internal Transcribed Spacer 1 (ITS1), where, together with Ltv1 and Tsr1, it coordinates stabilization of the pre-40S ribosomal beak structure in its immature conformation, facilitates repositioning of Rps3 (uS3), and late integration of Rps10 (eS10) (52–54,98). Due to its placement on the pre-40S subunit, it has also been suggested to play a role in the maturation of helix (h) 34 and the h34–h35–h38 three-way junction, which contain a central element in the formation of the A-site decoding center (h33/34), key residues for mRNA binding (h29–h32) and accommodation of anticodon-arms for all three tRNAs (h38–h42) (53,98,99). Loss of Enp1 results in early and late pre-rRNA processing and assembly defects causing accumulation of stalled 90S, pre-40S, and pre-60S ribosomes and their aberrant rRNA precursors, several of which become polyadenylated. However, here we show that instead of being degraded by the RNA exosome, which is functional in *enp1-1* cells, aberrant pre-rRNA precursors are bound by Nab2.

Out of more than 20 ribosome biogenesis mutants previously tested for a poly(A)-RNA accumulation defects (35), *enp1-1* was the only one in which a poly(A)-RNA accumulation phenotype was observed; however, many other ribosome biogenesis mutants are known to accumulate pre-

rRNAs (99,100). This suggests that the phenotypes observed in *enp1-1* cells are linked to specific Enp1 functions in ribosome maturation, in particular, late pre-40S ribosomes, since 23S, 21S/20S and 17S (but not 27SA/B) are polyadenylated and predominately enriched with Nab2 in *enp1-1* mutants. One possibility is that the absence of Enp1 leads to aberrant pre-rRNP conformations that cannot be efficiently degraded by the RNA exosome. The resulting pool of aberrant pre-rRNAs would engage and inhibit the RNA exosome, in turn leading to an accumulation of mRNAs, ncRNAs, and pervasive transcripts with Nab2 and other RBPs in the nucleolus that would normally be acted upon by the RNA exosome. Alternatively, defects in pre-rRNA processing caused by *enp1-1* may allow for Nab2 binding, which subsequently protects the pre-rRNAs from the RNA exosome complex and leads to Nab2 sequestration. This latter model would suggest an active role for Nab2 in RNA exosome inhibition through pre-rRNA binding.

Current structure-function and RNA-binding data indicate that Nab2 has a strong preference for polyadenine sequences (42,101), indicating that Nab2 recruitment to polyadenylated pre-rRNAs could initiate *enp1-1* phenotypes. However, Nab2 association with non-polyadenine sequences in the middle of mRNA transcripts has also been demonstrated (42,102), raising the possibility that Nab2 may as well bind other regions of pre-rRNAs and other RNAs. While 23S-containing pre-40S complexes are densely covered in protein (103), high-throughput rRNA structure probing (ChemModSeq) revealed that pre-40S particles containing Enp1 harbor a 3' major domain (corresponding to the beak and platform domains of the small ribosomal subunit) with a higher degree of flexibility (104). Moreover, the three-way junction formed by rRNA helices h34, h35 and h38 at the base of the head was shown to exist in an immature 'open' conformation (98,105). Thus it is conceivable that in the absence of functional Enp1 these open and flexible regions become stabilized, enabling cleavage of 23S at site Q1 (located within the central domain of the pre-18S rRNA) to generate aberrant 17S precursor (which are polyadenylated; Figure 4A) (26), but also leave rRNA regions exposed to binding of PABPs. We can therefore not rule out that Nab2 may also bind to non-polyadenylated regions of aberrant pre-rRNAs in these stalled complexes. Moreover, the majority of Nab2-associated U14 and snR30 snoRNAs were not polyadenylated, but whether this interaction occurs via Nab2 binding directly to the snoRNA or Nab2 and snoRNAs both associating with ribosome processing intermediates remains to be determined.

In either of these scenarios, the outcome is a build-up of nuclear and nucleolar mRNA and ncRNA containing RNPs in *enp1-1* cells that sequester RBPs as a result of the inability of the RNA exosome to process pre-rRNAs. The resulting excess of surveillance substrates is expected to inhibit RNA exosome functions leading to terminal phenotypes (e.g. snoRNA polyadenylation and pervasive transcript stabilization) that are similar to what is observed in RNA exosome mutants. A model that is supported by the correlated changes in the cellular transcriptome of *enp1-1*, *cs14-ph* and *dis3-1* strains involving mRNAs, pervasive transcripts and ncRNAs. Interestingly, a recent study in ag-

ing yeast cells also showed that an increase in pre-rRNA levels in the nucleolus fueled by the accumulation of extra-chromosomal rDNA resulted in a loss of nuclear homeostasis (106); however, the polyadenylation status of these pre-rRNAs or localization of PABPs were not investigated under these conditions.

Nuclear RNA homeostasis and disease

This work provides insight into potential interconnections between ncRNA processing, mRNA expression, and overall nuclear homeostasis. Speculatively, this type of mechanism may provide cells with a way to coordinate changes in mRNA and ncRNA transcript processing during periods that require rapid changes in gene expression (e.g. stress). Broadly, it is expected that investigating such concepts in *Saccharomyces cerevisiae* and other systems will aid our understanding of how mutations in essential RNA processing factors result in human disease. For example, mutations in the RNA exosome genes EXOSC3, EXOSC8 and EXOSC2 (RRP40, RRP43 and RRP4 in *S. cerevisiae*) or RNA exosome cofactors are known to cause tissue-specific diseases of varying phenotypes (107–110). Similarly, mutations in the PABP ZC3H14, a Nab2 ortholog, are associated with inherited intellectual disability (111). How mutations in these RNA surveillance and processing factors result in these particular diseases is not known. Various neurodegenerative diseases are also linked to altered RNA metabolism events, which in some instances have been shown to include the improper localization of RBPs (112,113). In addition, viral pathogens have more recently been found to modulate RNA exosome and RNA decay activities to both promote their own growth and evade host defense (114,115). Consequently, the phenotypes and molecular mechanisms observed in this work involving redistribution of PABPs, and RBPs more generally, may provide a rationale for further studies aimed at probing the molecular mechanisms at play in these and other disease states.

DATA AVAILABILITY

RNA-sequencing data is available using GEO accession numbers GSE134295. The mass spectrometry proteomics data have been deposited to the ProteomeXchange Consortium via the PRIDE (116) partner repository with the dataset identifier PXD021855 and Project DOI 10.6019/PXD021855. Code related to the analysis of the sequencing data and generation of each figure is available at https://github.com/montpetitlab/Aguiar_and_Paul_et_al_2020.

SUPPLEMENTARY DATA

Supplementary Data are available at NAR Online.

ACKNOWLEDGEMENTS

We would like to acknowledge Kelly Tedrick, Benedict Yong, Caitlin Porter, and Iris Unterweger, plus all past and current members of the Oeffinger and Montpetit laboratories for their support of this work. We also thank Dr Karsten Weis for strains used in this study and Dr Daniel Zenklusen for critical reading.

FUNDING

T.R. was supported by the Gordon and Betty Moore Foundation's Data-Driven Discovery Initiative [GBMF4551]; Harry Baccigaluppi Fellowship; Horace O Lanza Scholarship; Louis R Gombert Fellowship; Margrit Mondavi Fellowship; Haskell F Norman Wine & Food Fellowship; Chaîne des Rôtisseurs Scholarship; Carpenter Memorial Fellowship; AANR was funded by the predoctoral Training Program in Molecular and Cellular Biology at UC Davis that is supported by an NIH T32 [GM007377]; M.O. is a Fonds de recherche du Québec – Santé Boursier Chercheur Junior 2; Research reported in this publication was supported by the National Institute of General Medical Sciences of the National Institutes of Health [R01GM124120 to B.M.]; Canadian Institutes of Health Research [MOP 130231 to B.M., PJT 386315 to M.O.]; Infrastructure used to perform this work was supported by the W.M. Keck Foundation. The content is solely the responsibility of the authors and does not necessarily represent the views of the National Institutes of Health or other funding agencies. *Conflict of interest statement.* None declared.

REFERENCES

1. Singh, G., Pratt, G., Yeo, G.W. and Moore, M.J. (2015) The clothes make the mRNA: past and present trends in mRNP fashion. *Annu. Rev. Biochem.*, **84**, 325–354.
2. Matera, A.G., Terns, R.M. and Terns, M.P. (2007) Non-coding RNAs: lessons from the small nuclear and small nucleolar RNAs. *Nat. Rev. Mol. Cell Biol.*, **8**, 209–220.
3. Kressler, D., Hurt, E. and Baßler, J. (2017) A puzzle of life: crafting ribosomal subunits. *Trends Biochem. Sci.*, **42**, 640–654.
4. Hopper, A.K. and Huang, H.-Y. (2015) Quality control pathways for nucleus-encoded eukaryotic tRNA biosynthesis and subcellular trafficking. *Mol. Cell Biol.*, **35**, 2052–2058.
5. Peck, S.A., Hughes, K.D., Victorino, J.F. and Mosley, A.L. (2019) Writing a wrong: coupled RNA polymerase II transcription and RNA quality control. *Wiley Interdiscip. Rev. RNA*, **10**, e1529.
6. Schmid, M. and Jensen, T.H. (2019) The nuclear RNA exosome and its cofactors. In: *Advances in Experimental Medicine and Biology*. Vol. **1203**, pp. 113–132.
7. Porrua, O. and Libri, D. (2013) RNA quality control in the nucleus: the Angels' share of RNA. *Biochim. Biophys. Acta - Gene Regul. Mech.*, **1829**, 604–611.
8. Bresson, S. and Tollervey, D. (2018) Surveillance-ready transcription: nuclear RNA decay as a default fate. *Open Biol.*, **8**, 170270.
9. Chlebowski, A., Lubas, M., Jensen, T.H. and Dziembowski, A. (2013) RNA decay machines: the exosome. *Biochim. Biophys. Acta*, **1829**, 552–560.
10. Schneider, C. and Tollervey, D. (2013) Threading the barrel of the RNA exosome. *Trends Biochem. Sci.*, **38**, 485–493.
11. Allmang, C., Petfalski, E., Podtelejnikov, A., Mann, M., Tollervey, D. and Mitchell, P. (1999) The yeast exosome and human PM-Scl are related complexes of 3' right-arrow 5' exonucleases. *Genes Dev.*, **13**, 2148–2158.
12. Mitchell, P., Petfalski, E., Shevchenko, A., Mann, M. and Tollervey, D. (1997) The Exosome: a conserved eukaryotic RNA processing complex containing multiple 3' 5' exoribonucleases. *Cell*, **91**, 457–466.
13. Briggs, M.W., Burkard, K.T. and Butler, J.S. (1998) Rrp6p, the yeast homologue of the human PM-Scl 100-kDa autoantigen, is essential for efficient 5.8 S rRNA 3' end formation. *J. Biol. Chem.*, **273**, 13255–13263.
14. van Hoof, A., Lennertz, P. and Parker, R. (2000) Yeast exosome mutants accumulate 3'-extended polyadenylated forms of U4 small nuclear RNA and small nucleolar RNAs. *Mol. Cell Biol.*, **20**, 441–452.

15. Burkard, K.T. and Butler, J.S. (2000) A nuclear 3'-5' exonuclease involved in mRNA degradation interacts with Poly(A) polymerase and the hnRNA protein Npl3p. *Mol Cell Biol*, **20**, 604–616.
16. Vasiljeva, L. and Buratowski, S. (2006) Nrd1 interacts with the nuclear exosome for 3' processing of RNA polymerase II transcripts. *Mol. Cell*, **21**, 239–248.
17. Steinmetz, E.J., Conrad, N.K., Brow, D.A. and Corden, J.L. (2001) RNA-binding protein Nrd1 directs poly(A)-independent 3'-end formation of RNA polymerase II transcripts. *Nature*, **413**, 327–331.
18. de la Cruz, J., Kressler, D., Tollervey, D. and Linder, P. (1998) Dob1p (Mtr4p) is a putative ATP-dependent RNA helicase required for the 3' end formation of 5.8S rRNA in *Saccharomyces cerevisiae*. *EMBO J.*, **17**, 1128–1140.
19. Vanáčová, S., Wolf, J., Martin, G., Blank, D., Dettwiler, S., Friedlein, A., Langen, H., Keith, G. and Keller, W. (2005) A new yeast poly(A) polymerase complex involved in RNA quality control. *PLoS Biol.*, **3**, e189.
20. LaCava, J., Houseley, J., Saveanu, C., Petfalski, E., Thompson, E., Jacquier, A. and Tollervey, D. (2005) RNA degradation by the exosome is promoted by a nuclear polyadenylation complex. *Cell*, **121**, 713–724.
21. Wyers, F., Rougemaille, M., Badis, G., Rousselle, J.-C., Dufour, M.-E., Boulay, J., Régnauld, B., Devaux, F., Namane, A., Séraphin, B. *et al.* (2005) Cryptic pol II transcripts are degraded by a nuclear quality control pathway involving a new poly(A) polymerase. *Cell*, **121**, 725–737.
22. Schmidt, K. and Butler, J.S. (2013) Nuclear RNA surveillance: role of TRAMP in controlling exosome specificity. *Wiley Interdiscip. Rev. RNA*, **4**, 217–231.
23. Porrua, O. and Libri, D. (2015) Transcription termination and the control of the transcriptome: why, where and how to stop. *Nat. Rev. Mol. Cell Biol.*, **16**, 190–202.
24. Gudipati, R.K., Xu, Z., Lebreton, A., Séraphin, B., Steinmetz, L.M., Jacquier, A. and Libri, D. (2012) Extensive degradation of RNA precursors by the exosome in wild-type cells. *Mol. Cell*, **48**, 409–421.
25. Schneider, C., Kudla, G., Wlotzka, W., Tuck, A. and Tollervey, D. (2012) Transcriptome-wide analysis of exosome targets. *Mol. Cell*, **48**, 422–433.
26. Choque, E., Schneider, C., Gadai, O. and Dez, C. (2018) Turnover of aberrant pre-40S pre-ribosomal particles is initiated by a novel endonucleolytic decay pathway. *Nucleic Acids Res.*, **46**, 4699–4714.
27. Tudek, A., Porrua, O., Kabzinski, T., Lidschreiber, M., Kubicek, K., Fortova, A., Lacroute, F., Vanáčová, S., Cramer, P., Stefl, R. *et al.* (2014) Molecular basis for coordinating transcription termination with noncoding RNA degradation. *Mol. Cell*, **55**, 467–481.
28. Dez, C., Houseley, J. and Tollervey, D. (2006) Surveillance of nuclear-restricted pre-ribosomes within a subnucleolar region of *Saccharomyces cerevisiae*. *EMBO J.*, **25**, 1534–1546.
29. Wery, M., Ruidant, S., Schillewaert, S., Lepore, N., Lafontaine, D.L.J.J., Lepore, N. and Lafontaine, D.L.J.J. (2009) The nuclear poly(A) polymerase and exosome cofactor Trf5 is recruited cotranscriptionally to nucleolar surveillance. *RNA*, **15**, 406–419.
30. Houseley, J. and Tollervey, D. (2006) Yeast Trf5p is a nuclear poly(A) polymerase. *EMBO Rep.*, **7**, 205–211.
31. Carneiro, T., Carvalho, C., Braga, J., Rino, J., Milligan, L., Tollervey, D. and Carmo-Fonseca, M. (2007) Depletion of the yeast nuclear exosome subunit Rrp6 results in accumulation of polyadenylated RNAs in a discrete domain within the nucleolus. *Mol. Cell Biol.*, **27**, 4157–4165.
32. Kadaba, S., Wang, X. and Anderson, J.T. (2006) Nuclear RNA surveillance in *Saccharomyces cerevisiae*: Trf4p-dependent polyadenylation of nascent hypomethylated tRNA and an aberrant form of 5S rRNA. *RNA*, **12**, 508–521.
33. Lepore, N. and Lafontaine, D.L.J. (2011) A functional interface at the rDNA connects rRNA synthesis, pre-rRNA processing and nucleolar surveillance in budding yeast. *PLoS One*, **6**, e24962.
34. Grzechnik, P. and Kufel, J. (2008) Polyadenylation linked to transcription termination directs the processing of snoRNA precursors in yeast. *Mol. Cell*, **32**, 247–258.
35. Paul, B. and Montpetit, B. (2016) Altered RNA processing and export lead to retention of mRNAs near transcription sites and nuclear pore complexes or within the nucleolus. *Mol. Biol. Cell*, **27**, 2742–2756.
36. Davis, C.A. and Ares, M. (2006) Accumulation of unstable promoter-associated transcripts upon loss of the nuclear exosome subunit Rrp6p in *Saccharomyces cerevisiae*. *Proc. Natl. Acad. Sci. USA*, **103**, 3262–3267.
37. Schulz, D., Schwalb, B., Kiesel, A., Baejen, C., Torkler, P., Gagneur, J., Soeding, J. and Cramer, P. (2013) Transcriptome surveillance by selective termination of noncoding RNA synthesis. *Cell*, **155**, 1075–1087.
38. Van Dijk, E.L., Chen, C.L., Daubenton-Carafa, Y., Gourvennec, S., Kwapisz, M., Roche, V., Bertrand, C., Silvain, M., Legoix-Ne, P., Loeillet, S. *et al.* (2011) XUTs are a class of Xrn1-sensitive antisense regulatory non-coding RNA in yeast. *Nature*, **475**, 114–119.
39. Thiebaut, M., Kisseleva-Romanova, E., Rougemaille, M., Boulay, J. and Libri, D. (2006) Transcription termination and nuclear degradation of cryptic unstable transcripts: a role for the nrd1-nab3 pathway in genome surveillance. *Mol. Cell*, **23**, 853–864.
40. Arigo, J.T., Eyster, D.E., Carroll, K.L. and Corden, J.L. (2006) Termination of cryptic unstable transcripts is directed by yeast RNA-binding proteins Nrd1 and Nab3. *Mol. Cell*, **23**, 841–851.
41. Marquardt, S., Hazelbaker, D.Z. and Buratowski, S. (2011) Distinct RNA degradation pathways and 3' extensions of yeast non-coding RNA species. *Transcription*, **2**, 145–154.
42. Tuck, A.C. and Tollervey, D. (2013) A transcriptome-wide atlas of RNP composition reveals diverse classes of mRNAs and lncRNAs. *Cell*, **154**, 996–1009.
43. Sohrabi-Jahromi, S., Hofmann, K.B., Boltendahl, A., Roth, C., Gressel, S., Baejen, C., Soeding, J. and Cramer, P. (2019) Transcriptome maps of general eukaryotic RNA degradation factors. *Elife*, **8**, e47040.
44. Tudek, A., Schmid, M., Makaras, M., Barrass, J.D., Beggs, J.D. and Jensen, T.H. (2018) A nuclear export block triggers the decay of newly synthesized polyadenylated RNA. *Cell Rep.*, **24**, 2457–2467.
45. Schmid, M., Olszewski, P., Pelechano, V., Gupta, I., Steinmetz, L.M. and Jensen, T.H. (2015) The nuclear PolyA-binding protein Nab2p is essential for mRNA production. *Cell Rep.*, **12**, 128–139.
46. Green, D.M., Marfatia, K.A., Crafton, E.B., Zhang, X., Cheng, X. and Corbett, A.H. (2002) Nab2p is required for poly(A) RNA export in *Saccharomyces cerevisiae* and is regulated by arginine methylation via Hmt1p. *J. Biol. Chem.*, **277**, 7752–7760.
47. Hector, R.E., Nykamp, K.R., Dheur, S., Anderson, J.T., Non, P.J., Urbinati, C.R., Wilson, S.M., Minvielle-Sebastia, L. and Swanson, M.S. (2002) Dual requirement for yeast hnRNP Nab2p in mRNA poly(A) tail length control and nuclear export. *Embo J*, **21**, 1800–1810.
48. Dheur, S., Nykamp, K.R., Viphakone, N., Swanson, M.S. and Minvielle-Sebastia, L. (2005) Yeast mRNA poly(A) tail length control can be reconstituted in vitro in the absence of Pab1p-dependent poly(A) nuclease activity. *J. Biol. Chem.*, **280**, 24532–24538.
49. Reuter, L.M., Meinel, D.M. and Sträßer, K. (2015) The poly(A)-binding protein Nab2 functions in RNA polymerase III transcription. *Genes Dev.*, **29**, 1565–1575.
50. Kornprobst, M., Turk, M., Kellner, N., Cheng, J., Flemming, D., Koš-Braun, I., Koš, M., Thoms, M., Berninghausen, O., Beckmann, R. *et al.* (2016) Architecture of the 90S pre-ribosome: a structural view on the birth of the eukaryotic ribosome. *Cell*, **166**, 380–393.
51. Schäfer, T., Strauß, D., Petfalski, E., Tollervey, D. and Hurt, E. (2003) The path from nucleolar 90S to cytoplasmic 40S pre-ribosomes. *EMBO J.*, **22**, 1370–1380.
52. Schäfer, T., Maco, B., Petfalski, E., Tollervey, D., Böttcher, B., Aebi, U. and Hurt, E. (2006) Hrr25-dependent phosphorylation state regulates organization of the pre-40S subunit. *Nature*, **441**, 651–655.
53. Heuer, A., Thomson, E., Schmidt, C., Berninghausen, O., Becker, T., Hurt, E. and Beckmann, R. (2017) Cryo-EM structure of a late pre-40S ribosomal subunit from *Saccharomyces cerevisiae*. *Elife*, **6**, e30189.
54. Johnson, M.C., Ghalei, H., Doxtader, K.A., Karbstein, K. and Stroupe, M.E. (2017) Structural heterogeneity in pre-40S ribosomes. *Structure*, **25**, 329–340.
55. Amberg, D.C., Fleischmann, M., Stagljar, I., Cole, C.N. and Aebi, M. (1993) Nuclear PRP20 protein is required for mRNA export. *Embo J*, **12**, 233–241.

56. Gietz,R.D. and Woods,R.A. (2002) Transformation of yeast by lithium acetate/single-stranded carrier DNA/polyethylene glycol method. *Methods Enzymol.*, **350**, 87–96.
57. Oeffinger,M., Wei,K.E., Rogers,R., DeGrasse,J.A., Chait,B.T., Aitchison,J.D. and Rout,M.P. (2007) Comprehensive analysis of diverse ribonucleoprotein complexes. *Nat. Methods*, **4**, 951–956.
58. Schindelin,J., Arganda-Carreras,I., Frise,E., Kaynig,V., Longair,M., Pietzsch,T., Preibisch,S., Rueden,C., Saalfeld,S., Schmid,B. *et al.* (2012) Fiji: an open-source platform for biological-image analysis. *Nat. Methods*, **9**, 676–682.
59. Trahan,C. and Oeffinger,M. (2016) Targeted cross-linking-mass spectrometry determines vicinal interactomes within heterogeneous RNP complexes. *Nucleic Acids Res.*, **44**, 1354–1369.
60. Scott,D.D., Trahan,C., Zindy,P.J., Aguilar,L.C., Delubac,M.Y., Van Nostrand,E.L., Adivarahan,S., Wei,K.E., Yeo,G.W., Zenklusen,D. *et al.* (2017) Nol12 is a multifunctional RNA binding protein at the nexus of RNA and DNA metabolism. *Nucleic Acids Res.*, **45**, 12509–12528.
61. Patro,R., Duggal,G., Love,M.I., Irizarry,R.A. and Kingsford,C. (2017) Salmon provides fast and bias-aware quantification of transcript expression. *Nat. Methods*, **14**, 417–419.
62. Ellinger,M.A., Lederer,A.R., Warner,M.H., Mavrich,T.N., Raupach,E.A., Heisler,L.E., Nislow,C., Lee,M.T. and Arndt,K.M. (2019) The Paf1 complex broadly impacts the transcriptome of *Saccharomyces cerevisiae*. *Genetics*, **212**, 711–728.
63. Quinlan,A.R. (2014) BEDTools: The Swiss-Army tool for genome feature analysis. *Curr. Protoc. Bioinforma.*, **47**, doi:10.1002/0471250953.bi112s47.
64. Bolger,A.M., Lohse,M. and Usadel,B. (2014) Trimmomatic: a flexible trimmer for Illumina sequence data. *Bioinformatics*, **30**, 2114–2120.
65. Soneson,C., Love,M.I. and Robinson,M.D. (2015) Differential analyses for RNA-seq: transcript-level estimates improve gene-level inferences. *F1000Research*, **4**, 1521.
66. Love,M.I., Huber,W. and Anders,S. (2014) Moderated estimation of fold change and dispersion for RNA-seq data with DESeq2. *Genome Biol.*, **15**, 550.
67. Kim,D., Paggi,J.M., Park,C., Bennett,C. and Salzberg,S.L. (2019) Graph-based genome alignment and genotyping with HISAT2 and HISAT-genotype. *Nat. Biotechnol.*, **37**, 907–915.
68. Li,H., Handsaker,B., Wysoker,A., Fennell,T., Ruan,J., Homer,N., Marth,G., Abecasis,G., Durbin,R. and 1000 Genome Project Data Processing Subgroup (2009) The Sequence Alignment/Map format and SAMtools. *Bioinformatics*, **25**, 2078–2079.
69. Ramirez,F., Dündar,F., Diehl,S., Grüning,B.A. and Manke,T. (2014) deepTools: a flexible platform for exploring deep-sequencing data. *Nucleic Acids Res.*, **42**, W187–W191.
70. Bushnell,B. (2014) BMAP: a fast, accurate, splice-aware aligner. *Ernest Orlando Lawrence Berkeley Natl. Lab.*, <https://escholarship.org/uc/item/1h3515gn>.
71. Collart,M.A. and Oliviero,S. (1993) Preparation of Yeast RNA. *Curr. Protoc. Mol. Biol.*, **23**, 13.12.1–13.12.5.
72. Mansour,F.H. and Pestov,D.G. (2013) Separation of long RNA by agarose-formaldehyde gel electrophoresis. *Anal. Biochem.*, **441**, 18–20.
73. Lardenois,A., Liu,Y., Walther,T., Chalmel,F., Evrard,B., Granovskaia,M., Chu,A., Davis,R.W., Steinmetz,L.M. and Primig,M. (2011) Execution of the meiotic noncoding RNA expression program and the onset of gametogenesis in yeast require the conserved exosome subunit Rrp6. *Proc. Natl. Acad. Sci. U.S.A.*, **108**, 1058–1063.
74. Lemay,J.-F., D'Amours,A., Lemieux,C., Lackner,D.H., St-Sauveur,V.G., Bähler,J. and Bachand,F. (2010) The nuclear poly(A)-binding protein interacts with the exosome to promote synthesis of noncoding small nucleolar RNAs. *Mol. Cell*, **37**, 34–45.
75. Kim,M., Vasiljeva,L., Rando,O.J., Zhelkovsky,A., Moore,C. and Buratowski,S. (2006) Distinct pathways for snoRNA and mRNA termination. *Mol. Cell*, **24**, 723–734.
76. Heo,D., Yoo,I., Kong,J., Lidschreiber,M., Mayer,A., Choi,B.-Y., Hahn,Y., Cramer,P., Buratowski,S. and Kim,M. (2013) The RNA polymerase II C-terminal domain-interacting domain of yeast Nrd1 contributes to the choice of termination pathway and couples to RNA processing by the nuclear exosome. *J. Biol. Chem.*, **288**, 36676–36690.
77. Chen,W., Bucaria,J., Band,D.A., Sutton,A. and Sternglanz,R. (2003) Enp1, a yeast protein associated with U3 and U14 snoRNAs, is required for pre-rRNA processing and 40S subunit synthesis. *Nucleic Acids Res.*, **31**, 690–699.
78. McMahon,M.E., Stamenkovich,D. and Petes,T.D. (1984) Tandemly arranged variant 5S ribosomal RNA genes in the yeast *Saccharomyces cerevisiae*. *Nucleic Acids Res.*, **12**, 8001–8016.
79. Kuai,L., Fang,F., Butler,J.S. and Sherman,F. (2004) Polyadenylation of rRNA in *Saccharomyces cerevisiae*. *Proc. Natl. Acad. Sci. U.S.A.*, **101**, 8581–8586.
80. Zanchin,N.I.T. and Goldfarb,D.S. (1999) The exosome subunit Rrp43p is required for the efficient maturation of 5.8S, 18S and 25S rRNA. *Nucleic Acids Res.*, **27**, 1283–1288.
81. Allmang,C., Mitchell,P., Petfalski,E. and Tollervey,D. (2000) Degradation of ribosomal RNA precursors by the exosome. *Nucleic Acids Res.*, **28**, 1684–1691.
82. Zhang,J., Harnpicharnchai,P., Jakovljevic,J., Tang,L., Guo,Y., Oeffinger,M., Rout,M.P., Hiley,S.L., Hughes,T. and Woolford,J.L. (2007) Assembly factors Rpf2 and Rrs1 recruit 5S rRNA and ribosomal proteins rpl5 and rpl11 into nascent ribosomes. *Genes Dev.*, **21**, 2580–2592.
83. Grandi,P., Rybin,V., Baßler,J., Petfalski,E., Strauß,D., Marzoch,M., Schäfer,T., Kuster,B., Tschochner,H., Tollervey,D. *et al.* (2002) 90S pre-ribosomes include the 35S pre-rRNA, the U3 snoRNP, and 40S subunit processing factors but predominantly lack 60S synthesis factors. *Mol. Cell*, **10**, 105–115.
84. Losh,J.S., King,A.K., Bakelar,J., Taylor,L., Loomis,J., Rosenzweig,J.A., Johnson,S.J. and van Hoof,A. (2015) Interaction between the RNA-dependent ATPase and poly(A) polymerase subunits of the TRAMP complex is mediated by short peptides and important for snoRNA processing. *Nucleic Acids Res.*, **43**, 1848–1858.
85. Loewith,R. and Hall,M.N. (2011) Target of rapamycin (TOR) in nutrient signaling and growth control. *Genetics*, **189**, 1177–1201.
86. Delan-Forino,C., Spanos,C., Rappsilber,J. and Tollervey,D. (2020) Substrate specificity of the TRAMP Nuclear Surveillance Complexes. *Nat. Commun.*, **11**, 3122.
87. Aitchison,J.D., Blobel,G. and Rout,M.P. (1996) Kap104p: a karyopherin involved in the nuclear transport of messenger RNA binding proteins. *Science (80-)*, **274**, 624–627.
88. Tudek,A., Lloret-Llinares,M. and Jensen,T.H. (2018) The multitasking poly(A) tail: nuclear RNA maturation, degradation and export. *Philos. Trans. R. Soc. B Biol. Sci.*, **373**, 20180169.
89. Tian,B. and Manley,J.L. (2017) Alternative polyadenylation of mRNA precursors. *Nat. Rev. Mol. Cell Biol.*, **18**, 18–30.
90. Edmonds,M. (2002) A history of poly A sequences: from formation to factors to function. *Prog. Nucleic Acid Res. Mol. Biol.*, **71**, 285–389.
91. Goss,D.J. and Kleiman,F.E. (2013) Poly(A) binding proteins: are they all created equal? *Wiley Interdiscip. Rev. RNA*, **4**, 167–179.
92. Brambilla,M., Martani,F., Bertacchi,S., Vitangeli,I. and Branduardi,P. (2019) The *Saccharomyces cerevisiae* poly(A) binding protein (Pab1): master regulator of mRNA metabolism and cell physiology. *Yeast*, **36**, 23–34.
93. Soucek,S., Corbett,A.H. and Fasken,M.B. (2012) The long and the short of it: the role of the zinc finger polyadenosine RNA binding protein, Nab2, in control of poly(A) tail length. *Biochim. Biophys. Acta - Gene Regul. Mech.*, **1819**, 546–554.
94. Mangus,D.A., Evans,M.C. and Jacobson,A. (2003) Poly(A)-binding proteins: multifunctional scaffolds for the post-transcriptional control of gene expression. *Genome Biol.*, **4**, 223.
95. Perumal,K. and Reddy,R. (2002) The 3' end formation in small RNAs. *Gene Expr.*, **10**, 59–78.
96. Carmody,S.R., Tran,E.J., Apponi,L.H., Corbett,A.H. and Wente,S.R. (2010) The mitogen-activated protein kinase Slt2 regulates nuclear retention of non-heat shock mRNAs during heat shock-induced stress. *Mol. Cell Biol.*, **30**, 5168–5179.
97. Villa,T., Barucco,M., Martin-Niclos,M.-J., Jacquier,A. and Libri,D. (2020) Degradation of non-coding RNAs promotes recycling of termination factors at sites of transcription. *Cell Rep.*, **21**, 107942.
98. Shayan,R., Rinaldi,D., Larburu,N., Plassart,L., Balor,S., Bouysié,D., Lebaron,S., Marcoux,J., Gleizes,P.-E. and Plisson-Chastang,C. (2020) Good Vibrations: Structural remodeling

- of maturing yeast Pre-40S ribosomal particles followed by Cryo-Electron microscopy. *Molecules*, **25**, 1125.
99. Cerezo, E., Plisson-Chastang, C., Henras, A.K., Lebaron, S., Gleizes, P., O'Donohue, M., Romeo, Y. and Henry, Y. (2019) Maturation of pre-40S particles in yeast and humans. *Wiley Interdiscip. Rev. RNA*, **10**, e1516.
 100. Henras, A.K., Plisson-Chastang, C., O'Donohue, M.F., Chakraborty, A. and Gleizes, P.E. (2015) An overview of pre-ribosomal RNA processing in eukaryotes. *Wiley Interdiscip. Rev. RNA*, **6**, 225–242.
 101. Fasken, M.B., Corbett, A.H. and Stewart, M. (2019) Structure-function relationships in the Nab2 polyadenosine-RNA binding Zn finger protein family. *Protein Sci.*, **28**, 513–523.
 102. Viphakone, N., Voisiniet-Hakil, F. and Minvielle-Sebastia, L. (2008) Molecular dissection of mRNA poly(A) tail length control in yeast. *Nucleic Acids Res.*, **36**, 2418–2433.
 103. Barandun, J., Hunziker, M. and Klinge, S. (2018) Assembly and structure of the SSU processome — a nucleolar precursor of the small ribosomal subunit. *Curr. Opin. Struct. Biol.*, **49**, 85–93.
 104. Hector, R.D., Burlacu, E., Aitken, S., Bihan, T.Le, Tuijtel, M., Zaplatina, A., Cook, A.G. and Granneman, S. (2014) Snapshots of pre-rRNA structural flexibility reveal eukaryotic 40S assembly dynamics at nucleotide resolution. *Nucleic Acids Res.*, **42**, 12138–12154.
 105. Mitterer, V., Shayan, R., Ferreira-Cerca, S., Murat, G., Enne, T., Rinaldi, D., Weigl, S., Omani, H., Gleizes, P.E., Kressler, D. *et al.* (2019) Conformational proofreading of distant 40S ribosomal subunit maturation events by a long-range communication mechanism. *Nat. Commun.*, **10**, 2754.
 106. Morlot, S., Song, J., Léger-Silvestre, I., Matifas, A., Gadal, O. and Charvin, G. (2019) Excessive rDNA transcription drives the disruption in nuclear homeostasis during entry into senescence in budding yeast. *Cell Rep.*, **28**, 408–422.
 107. Morton, D.J., Kuiper, E.G., Jones, S.K., Leung, S.W., Corbett, A.H. and Fasken, M.B. (2018) The RNA exosome and RNA exosome-linked disease. *RNA*, **24**, 127–142.
 108. Fabre, A., Charroux, B., Martinez-Vinson, C., Roquelaure, B., Odul, E., Sayar, E., Smith, H., Colomb, V., Andre, N., Hugot, J.P. *et al.* (2012) SKIV2L mutations cause syndromic diarrhea, or trichohepatoenteric syndrome. *Am. J. Hum. Genet.*, **90**, 689–692.
 109. Giunta, M., Edvardson, S., Xu, Y., Schuelke, M., Gomez-Duran, A., Boczonadi, V., Elpeleg, O., Müller, J.S. and Horvath, R. (2016) Altered RNA metabolism due to a homozygous RBM7 mutation in a patient with spinal motor neuropathy. *Hum. Mol. Genet.*, **25**, 2985–2996.
 110. Hartley, J.L., Zachos, N.C., Dawood, B., Donowitz, M., Forman, J., Pollitt, R.J., Morgan, N.V., Tee, L., Gissen, P., Kahr, W.H.A. *et al.* (2010) Mutations in TTC37 cause trichohepatoenteric syndrome (Phenotypic Diarrhea of Infancy). *Gastroenterology*, **138**, 2388–2398.
 111. Pak, C.H., Garshasbi, M., Kahrizi, K., Gross, C., Apponi, L.H., Noto, J.J., Kelly, S.M., Leung, S.W., Tzschach, A., Behjati, F. *et al.* (2011) Mutation of the conserved polyadenosine RNA binding protein, ZC3H14/dNab2, impairs neural function in *Drosophila* and humans. *Proc. Natl. Acad. Sci. U.S.A.*, **108**, 12390–12395.
 112. Volkening, K. and Strong, M.J. (2011) RNA Metabolism in neurodegenerative disease. *Curr. Chem. Biol.*, **5**, 90–98.
 113. Droppelmann, C.A., Campos-Melo, D., Ishtiaq, M., Volkening, K. and Strong, M.J. (2014) RNA metabolism in ALS: When normal processes become pathological. *Amyotroph. Lateral Scler. Front. Degener.*, **15**, 321–336.
 114. Guo, L., Louis, I.V.S. and Bohjanen, P.R. (2018) Viral manipulation of host mRNA decay. *Future Virol.*, **13**, 211–223.
 115. Rialdi, A., Hultquist, J., Jimenez-Morales, D., Peralta, Z., Campisi, L., Fenouil, R., Moshkina, N., Wang, Z.Z., Laffleur, B., Kaake, R.M. *et al.* (2017) The RNA exosome syncs IAV-RNAPII transcription to promote viral ribogenesis and infectivity. *Cell*, **169**, 679–692.
 116. Perez-Riverol, Y., Csordas, A., Bai, J., Bernal-Llinares, M., Hewapathirana, S., Kundu, D.J., Inuganti, A., Griss, J., Mayer, G., Eisenacher, M. *et al.* (2019) The PRIDE database and related tools and resources in 2019: improving support for quantification data. *Nucleic Acids Res.*, **47**, D442–D450.